Strathprints Institutional Repository

Cardona, Javier and Fartaria, Rui and Sweatman, Martin B. and Lue, Leo (2016) Molecular dynamics simulations for the prediction of the dielectric spectra of alcohols, glycols, and monoethanolamine. Molecular Simulation, 42 (5). pp. 370-390. ISSN 0892-7022 , http://dx.doi.org/10.1080/08927022.2015.1055741

This version is available at http://strathprints.strath.ac.uk/54062/

Strathprints is designed to allow users to access the research output of the University of Strathclyde. Unless otherwise explicitly stated on the manuscript, Copyright © and Moral Rights for the papers on this site are retained by the individual authors and/or other copyright owners. Please check the manuscript for details of any other licences that may have been applied. You may not engage in further distribution of the material for any profitmaking activities or any commercial gain. You may freely distribute both the url (http://strathprints.strath.ac.uk/) and the content of this paper for research or private study, educational, or not-for-profit purposes without prior permission or charge.

Any correspondence concerning this service should be sent to Strathprints administrator: strathprints@strath.ac.uk

Molecular Simulation
Vol. 00, No. 00, Month 2009, 1–22

RESEARCH ARTICLE

Molecular dynamics simulations for the prediction of the dielectric spectra of alcohols, glycols, and monoethanolamine

Javier Cardona[a] *, Rui Fartaria[b] , Martin B. Sweatman[b] and Leo Lue[a]

[a]*Department of Chemical and Process Engineering, University of Strathclyde, James Weir Building, 75 Montrose Street, Glasgow G1 1XJ, United Kingdom*; [b]*School of Engineering, The University of Edinburgh, The King's Buildings, Sanderson Building, Mayfield Road, Edinburgh, EH9 3JL, United Kingdom*

(*v4.3 released January 2009*)

The response of molecular systems to electromagnetic radiation in the microwave region (0.3–300 GHz) has been principally studied experimentally, using broadband dielectric spectroscopy. However, relaxation times corresponding to reorganisation of molecular dipoles due to their interaction with electromagnetic radiation at microwave frequencies are within the scope of modern molecular simulations. In this work, fluctuations of the total dipole moment of a molecular system, obtained through molecular dynamics simulations, are used to determine the dielectric spectra of water, a series of alcohols and glycols, and monoethanolamine. Although the force fields employed in this study have principally been developed to describe thermodynamic properties, most them give fairly good predictions of this dynamical property for these systems. However, the inaccuracy of some models and the long simulation times required for the accurate estimation of the static dielectric constant can sometimes be problematic. We show that the use of the experimental value for the static dielectric constant in the calculations, instead of the one predicted by the different models, yields satisfactory results for the dielectric spectra, and hence the heat absorbed from microwaves, avoiding the need for extraordinarily long simulations or re-calibration of molecular models.

Keywords: dielectric spectra; microwaves; molecular dynamics; alcohols; monoethanolamine

1 Introduction

Microwave heating arises from the coupling of charges in dielectric media to an electromagnetic field. In molecular systems, molecular dipoles reorganize in an attempt to align themselves with the oscillating electric field. However, the resulting motions are often impeded by collisions between molecules, and, consequently, the charges are not always able to keep up with the rate at which the field oscillates in the microwave region (0.3–300 GHz) and a lag is observed. This delay or relaxation in the molecular response with respect to the application of the electric field provides the origin of the conversion of electromagnetic energy into thermal energy in microwave heating. At lower frequencies, the dipoles are able to remain in phase with the electric field and no major variation is observed in the temperature of the irradiated material. At higher frequencies, the dipoles are not fast enough to follow the rapid oscillations of the electric field [1]. In this case, absorption takes place through electronic degrees of freedom.

The dielectric properties of the material dictate its tendency to convert electromagnetic energy into thermal energy. This is reflected in the definition of the dielectric permittivity $\hat{\varepsilon}(\omega)$ as a

*Corresponding author. Email: j.cardona-amengual@strath.ac.uk

ISSN: 0892-7022 print/ISSN 1029-0435 online
© 2009 Taylor & Francis
DOI: 10.1080/0892702YYxxxxxxxx
http://www.informaworld.com

For Peer Review Only

complex frequency-dependent quantity given by:

$$\hat{\varepsilon}(\omega) = \varepsilon'(\omega) + i\,\varepsilon''(\omega) \tag{1}$$

where $\varepsilon'(\omega)$ is the real part of the complex dielectric permittivity and represents the ability of a material to store potential energy due to polarization by an electric field, while $\varepsilon''(\omega)$ is the imaginary part of the complex dielectric permittivity or dielectric loss, and represents its ability to transform the absorbed energy into heat.

One of the simplest models used to describe dielectric relaxation was suggested by Debye [2]. According to the Debye model, the different dipoles forming the dielectric medium interact with each other only through random collisions, captured through a relaxation time, and the resulting complex dielectric permittivity is given by:

$$\hat{\varepsilon}(\omega) = \varepsilon_\infty + \frac{\varepsilon_0 - \varepsilon_\infty}{1 + i\,\omega\tau_D} \tag{2}$$

where ε_∞ is the infinite frequency dielectric constant, ε_0 is the static or zero-frequency dielectric constant, and τ_D is the dielectric relaxation time. This expression is generally valid for gases and liquids formed by small molecules. More complicated representations (e.g., Cole-Cole [3], Cole-Davidson [4], or Havriliak-Negami [5] models) are typically necessary to describe the dielectric behavior of higher molecular weight systems, such as polymers.

The study of microwave heating processes at a larger scale requires the resolution of an energy balance in which the heat absorbed by a dielectric material in a microwave field has to be considered. This term mainly depends on the dielectric properties of the material and the characteristics of the field [1]:

$$\dot{Q}_{abs} = \frac{\omega}{4\pi}\,\varepsilon''(\omega)\,|\mathbf{E}|^2\,V \tag{3}$$

where ω is the angular frequency of the electromagnetic field, $\mathbf{E}$ represents the electric field strength and V is the volume of the system.

Applications of microwave heating are rapidly growing, as its volumetric effect can lead to faster heat transfer in comparison with conventional conductive heating methods. One of the fields in which microwave heating is having a high impact is organic synthesis. Some of the most recent applications in this area have been summarized by de la Hoz and Loupy [6]. Another interesting aspect is the development of techniques based on dielectric properties to study the conformation and dynamics of molecular systems. Kremer and Schönhals [7] provide a review on recent advances in broadband dielectric spectroscopy, including applications in the analysis of the molecular dynamics of glasses, supercooled fluids and polymers.

The dielectric characteristics of pure water and aqueous solutions are, for obvious reasons, among the most studied. Using dielectric spectroscopy, it has been shown that, in liquid water, dipole rotation translates into a so called α-relaxation process which clearly exhibits simple Debye behaviour in the microwave region over a wide range of temperatures [8–11], despite the presence of hydrogen bonding. The effect of adding different solutes on the strength of this hydrogen bonding network has also been analysed for various aqueous solutions [12]. Short alcohols start to show small deviations from the ideal Debye behavior at high frequencies, while the deviation in larger alcohols is more significant. The hydroxyl groups in alcohols can relax freely in the gas phase, but the presence of hydrogen bonding in the liquid phase limits the rotation of these groups [6]. This is signaled by the appearance of multiple absorption regions [13–17] in the dielectric absorption spectra. A similar effect has been observed in water/ethanol mixtures, which show a distribution of relaxation times, as opposed to the single peaks observed for the pure components [18].

Despite the relatively large literature on microwave heating and dielectric spectroscopy, the

For Peer Review Only

majority of the work in this area has been experimental, while there is relatively little computational work. Nevertheless, Rick, Stuart, and Berne [19] and later English and MacElroy [20, 21] determined the dielectric spectrum of water via equilibrium molecular dynamics simulations using the relationship between dipole moment fluctuations and the frequency-dependent dielectric constant initially developed by Neumann and Steinhauser [22, 23]. Non-equilibrium molecular dynamics simulations have also been performed in order to model the microwave heating of water [24–26], and the effects of an external electromagnetic field on the conductivity of molten sodium chloride [27], rutile TiO_2 [28], nanoconfined fluids [29] and binary dimethylimidazolium-based ionic liquid/water solutions [30–33]. Additionally, recent work has been carried out on dielectric spectroscopy of more complex systems such as protein solutions [34–36]. The paucity of simulation work can probably be explained by the fact that usual relaxation times corresponding to the reorganization of molecular dipoles due to their interaction with electromagnetic radiation at microwaves frequencies are on the order of nanoseconds, or even microseconds for larger molecules. This requires long, computationally expensive simulations in order to obtain statistically accurate results. Another cause for this scarcity in simulation work could be that most atomistic force fields for molecular simulations have been developed to reproduce thermodynamic rather than dynamic properties. Thus, it is unclear how reliably they will be able to reproduce the dynamic dielectric properties of a material.

In this work, we examine the ability of several different force fields to reproduce the dielectric spectra of relatively small molecules, such as water, alcohols, glycols and monoethanolamine (MEA). In order to do so, we perform equilibrium molecular dynamics simulations for those systems, and apply the methodology developed by Neumann and Steinhauser to obtain their frequency-dependent complex permittivity. Ultimately, our aim is to apply the results of this work to the application of microwaves in regenerating spent adsorbent materials. Equations 1 to 3 indicate this requires good prediction of the dielectric spectra of the materials involved in the process, including the static dielectric constant. In particular, our interest is mainly focused on the regeneration of impregnated materials used for carbon capture within the scope of a 'Wetting Layer Absorption (WLA)' process [37, 38]. This process employs solid adsorbents impregnated with amine compounds to capture carbon dioxide, hence, the inclusion of MEA in this study.

The remainder of this paper is organized as follows. The following section gives the details of the potential models used to describe the different molecules and explains the methodology employed to obtain their dielectric spectra. The results of the simulations are presented and discussed in Sec. 3. We find that the force fields examined in this work show generally good predictions of dielectric spectra. The estimation of the static dielectric constant can sometimes be problematic though, due to the inaccuracy of some models and the long simulation times required. In this study, we obtain satisfactory results by employing the experimental value of this parameter in our calculations, instead of the one predicted by the models. This improves the prediction of dielectric spectra while significantly reducing the simulation times required, and hence, will result in more realistic estimations of the heat a dielectric material can absorb from microwaves. Finally, in Sec. 4, we summarize the main findings of the work and provide directions for future studies.

2 Methodology

In this section, we present the force fields used to describe the molecular systems examined in this paper. In addition, we give details of the simulations and calculations performed, in particular, the method for calculating the dielectric spectrum.

For Peer Review Only

2.1 *Molecular models and interactions*

In this work, we analyse water, a series of alcohols and glycols (i.e. ethanol, ethylene glycol, propylene glycol, and glycerol), and monoethanolamine (MEA). For water, three rigid models (SPC [39], TIP4P [40], and SPC/E [41]) and two flexible models (F-SPC [42] and Fw-SPC [43]) are examined. For the alcohols and glycols, three force fields are used: Transferable Potentials for Phase Equilibria - United Atom [44, 45] (TraPPE-UA), Optimized Potentials for Liquid Simulations [46, 47] (OPLS) and Generalized Amber Force Field [47, 48] (GAFF). Finally, to model MEA we use the MEAa force field [49] along with the transferable OPLS and GAFF force fields. In the following, we summarize the main characteristics of the different force fields. The parameters used in our simulations are mainly taken from the original papers for each force field, and their values can be found in the appendix.

Nonbonded interactions

Nonbonded interactions between atoms are represented as the sum of a Lennard-Jones (LJ) 12-6 pair potential and an electrostatic interaction:

$$U_{nb}(r_{ij}) = 4\epsilon_{ij}\left[\left(\frac{\sigma_{ij}}{r_{ij}}\right)^{12} - \left(\frac{\sigma_{ij}}{r_{ij}}\right)^{6}\right] + \frac{q_i q_j}{4\pi\varepsilon_{vac} r_{ij}} \tag{4}$$

where r_{ij} is the distance between the atoms i and j, ϵ_{ij} is the depth of the potential well, and σ_{ij} is the distance at which the LJ potential is zero. In the second term, q_i and q_j are the charges of atoms i and j, respectively, and $\varepsilon_{vac} = 8.85418782 \times 10^{-12}\,\mathrm{F\,m^{-1}}$ is the vacuum permittivity. Nonbonded interactions apply to all intermolecular interactions, but, for intramolecular interactions, they only apply to atoms separated by three or more bonds. This varies, depending on the model, as discussed below.

The Lorentz-Berthelot combination rules are used in the TraPPE-UA, GAFF and MEAa force fields to calculate the interatomic parameters ϵ_{ij} and σ_{ij} from the atomic parameters ϵ_i and σ_i:

$$\begin{aligned} \sigma_{ij} &= \frac{1}{2}(\sigma_i + \sigma_j) \\ \epsilon_{ij} &= (\epsilon_i \epsilon_j)^{1/2}. \end{aligned} \tag{5}$$

Alternatively, the OPLS force field employs a geometric average:

$$\begin{aligned} \sigma_{ij} &= (\sigma_i \sigma_j)^{1/2} \\ \epsilon_{ij} &= (\epsilon_i \epsilon_j)^{1/2}. \end{aligned} \tag{6}$$

Bonded interactions

Bond stretching interactions between atoms separated by one bond are modelled by means of a harmonic potential:

$$U_b(r_{ij}) = \frac{1}{2}k_b(r_{ij} - b_0)^2 \tag{7}$$

where k_b is the spring constant bond, and b_0 is the equilibrium bond length. This applies only to bonds in the F-SPC and Fw-PSC water models, and the MEAa force field, because the remaining molecular models use rigid bonds with a fixed bond length b_0.

Similarly to the bond stretching potential, bending of the angle between two adjacent bonds

For Peer Review Only

can be represented using a harmonic potential:

$$U_a(\theta) = \frac{1}{2} k_\theta (\theta - \theta_0)^2 \tag{8}$$

where k_θ is the spring constant for bond angle bending, and θ_0 is the equilibrium bond angle.

The last of the bonded interactions considered in most of the models is the internal molecular torsion. In the force fields employed in this work, the potential related to the dihedral angle between four consecutive atoms in a molecule is described either by a Ryckaert-Bellemans or a Fourier function:

Ryckaert-Bellemans dihedral:

$$U_d(\phi) = \sum_{n=0}^{3} c_n \cos^n(\phi - 180^\circ) \tag{9}$$

where ϕ is the dihedral angle (zero-cis convention), and c_n are the different constants defining the model.

Fourier dihedral:

$$\begin{aligned} U_d(\phi) = \frac{1}{2} [C_1 (1 + \cos(\phi)) + C_2 (1 - \cos(2\phi)) \\ + C_3 (1 + \cos(3\phi))] \end{aligned} \tag{10}$$

where ϕ is the dihedral angle (zero-cis convention), and C_n are the different constants defining the model.

Particularities of the molecular models

We analyse the performance of five of the most common water models: the simple point charge (SPC) model [39], the TIP4P model [40], the SPC/E model [41], the Flexible SPC (F-SPC) model [42] and the Fw-SPC model [43] (see Fig. 1). More details on the models can be found in the appendix. The rationale behind the selection of these particular water models was not that of performing an exhaustive study on the dielectric properties of water, which have already been analysed extensively. We rather want to compare our results with previous simulation work [20, 21] in order to validate our methods and extend those to additional systems.

For the remaining molecules, more generalized force fields are used. The Transferable Potentials for Phase Equilibria (TraPPE) force field is parameterised to describe phase equilibrium and structural properties of a wide range of compounds. Its United Atom version (TraPPE-UA) [44, 45] is used to model ethanol, ethylene glycol and propylene glycol. While the first two molecules have been tested by the original authors, there is no evidence of previous work carried out with propylene glycol. Therefore, based on TraPPE parameters, we decided to build our own TraPPE-UA model for propylene glycol. Glycols require a repulsive potential of the form:

$$U_{rep}(r_{ij}) = \frac{a}{r_{ij}^{12}}, \tag{11}$$

between hydroxyl hydrogens and oxygens situated four bonds away, where $a = 6.2 \times 10^{-7}$ kJ mol^{-1} nm^{12}. This is needed to avoid the hydrogen atom, not originally protected by a LJ potential, overlapping the oxygen atom which has an opposite charge and will tend to attract it. Both OPLS [46, 47] and GAFF [47, 48] force fields are all-atom models which consider alkyl hydrogens explicitly. In this work, they have been used to model every studied compound (except water), although model parameters for ethylene and propylene glycols could not be found in the literature and so their topologies are built based on similar molecules (ethanol and glycerol). Finally the MEAa [49] force field is again an all-atom model. It is mainly based on

For Peer Review Only

GAFF's MEA model but some corrections were introduced in the charge distribution, the bond flexibility and the O-C-C-N, C-C-O-H and C-C-N-H dihedrals, in order to improve the prediction of intramolecular interactions, which are believed to have an important effect on the properties of MEA in the liquid phase.

The 1-4 nonbonded interactions are treated differently by the various force fields. The TraPPE-UA model generally excludes these interactions, but in the particular case of ethylene and propylene glycol, coulombic interactions between atoms separated by three bonds are included, although scaled by a factor of 0.5. OPLS, GAFF and MEAa force fields include both LJ and coulombic 1-4 interactions with different scaling factors. The OPLS model only considers half of the magnitude of these interactions. The same strategy is used by the GAFF force field regarding LJ interactions, however, coulombic interactions are scaled by a factor of 5/6 in this case. Finally MEAa fully considers all 1-4 nonbonded interactions.

Figure 1 shows the distribution of charges and LJ interaction sites for the models under consideration. As mentioned previously, the parameters defining the different molecular interactions used in our simulations can be found in the appendix.

2.2 *Simulation details*

Molecular dynamics (MD) simulations are carried out using the GROMACS 4.6.3 [50] package to study the performance of the different force fields in the prediction of dielectric spectra. All the systems consist of simulation boxes containing 1000 molecules and are simulated for 25 to 100 ns, depending on the time required to obtain a converged value for the static dielectric constant. Starting from independent and equilibrated configurations, four simulations are carried out for every molecular system, and the results are averaged across those four samples. The equations of motion are integrated by means of the leap-frog algorithm [51] with a time step of 1 fs for rigid (SPC, TIP4P, and SPC/E) and semi-flexible models (TraPPE-UA, OPLS and GAFF), and 0.2 fs for flexible force fields (F-SPC, Fw-SPC and MEAa). The trajectory of the molecules is read every 100 fs while the energy configuration is recorded every 50 fs. The simulations are performed with the NPT ensemble at 298 K and 1 bar, except for MEA for which a temperature of 293 K is used due to the larger availability of experimental data at that temperature. The Nosé-Hoover thermostat [52, 53], with a time constant of 0.1 ps, is used for temperature coupling while the pressure is controlled by means of a Parrinello-Rahman barostat [54, 55] with a compressibility of $4.5 \times 10^{-5}\,\mathrm{bar}^{-1}$ and a time constant of 1.0 ps. The LINCS algorithm [56] is responsible for constraining the bond length when necessary. A cut-off radius of 0.85 nm is used for the Lennard-Jones interactions in all the systems, except when the TraPPE-UA or the MEAa force fields are used; for those models, the LJ interaction is truncated at 1.40 nm and 1.00 nm, respectively. Long-range electrostatics are treated with the particle mesh Ewald (PME) method [57] with a truncation at the same distance as the LJ one, and a spacing for the PME grid of 0.12 nm. Analytical tail corrections in potential energy are used to compensate for the truncation in LJ interactions. Finally, cubic and conducting periodic boundary conditions are used in every case.

2.3 *Determination of the frequency-dependent dielectric constant*

The total dipole moment $\mathbf{M}$ of a polar system corresponds to the sum of the individual dipole moments $\boldsymbol{\mu}_i$ of each of the molecules in the system (i.e. $\mathbf{M} = \sum_i^N \boldsymbol{\mu}_i$). A time series of this quantity can be determined by molecular dynamics simulation. The fluctuations of the dipole moment can be directly related to the frequency dependent dielectric response [22]:

$$\frac{\hat{\varepsilon}(\omega) - \varepsilon_\infty}{\varepsilon_0 - \varepsilon_\infty} = 1 + i\omega\,\hat{\phi}(\omega) \tag{12}$$

For Peer Review Only

where $\hat{\phi}(\omega)$ is the Fourier transform of the total dipole moment autocorrelation function $\phi(t)$, which is given by:

$$\phi(t) = \frac{\langle \mathbf{M}(t) \cdot \mathbf{M}(0) \rangle}{\langle \mathbf{M}(0) \cdot \mathbf{M}(0) \rangle}. \tag{13}$$

As defined previously, ε_∞ is the infinite frequency relative permittivity (1 for non-polarizable potential models), and ε_0 is the zero-frequency or static dielectric constant.

To determine the frequency-dependent dielectric constant from Eq. (12), it is necessary to obtain the Fourier transform of the dipole moment autocorrelation function $\phi(t)$. In order to obtain this from a finite duration MD simulation, $\phi(t)$ is represented as the sum of a short time contribution $y_{cub}(t)$ and a long term exponential decay $y_{exp}(t)$ (i.e. $\phi(t) = y_{cub}(t) + y_{exp}(t)$). The short-time oscillatory portion of the autocorrelation function is fitted with a cubic spline through the initial range of discretely sampled points, and its Fourier transform is obtained analytically [19, 20]. For long times, the dipole moment autocorrelation function is fitted to an exponential decay:

$$y_{exp}(t) = Ae^{-t/\tau_D} \tag{14}$$

in-line with the Debye model, where τ_D is the relaxation time of the exponential decay. The exponential fit was only performed in the region where such a trend was clearly observed, and the same criterion was used for all the systems. This varies for the different models as they show different behaviour. However, we used the same fitting window for the four different runs corresponding to the same model.

3 Results and Discussion

3.1 *Thermodynamic properties*

Table 1 summarizes several thermodynamic properties for the systems we study, as determined [47, 58] from the molecular dynamics simulations.

Although thermodynamic properties are not the main focus of this work, we provide these results as a benchmark for the validity of our simulations. The standard errors for the different properties are obtained by averaging across the values obtained for each of the four independent simulations for every system. Most of the force fields used in this study are developed for the prediction of thermodynamic properties. Therefore, as expected, the results are generally in good agreement with experimental data. These are also consistent with previous simulation work by Caleman and coworkers [47], where the overprediction of the heat capacities is also observed and thought to be due to the neglect of quantum corrections in the calculation of enthalpy fluctuations.

3.2 *Dielectric and dynamic properties*

3.2.1 Summary of dielectric and dynamic properties

Table 2 summarizes the results obtained for the dielectric properties of the compounds, along with additional dynamic properties. The self-diffusion coefficient D is derived from the mean squared displacement of the positions of the atoms. The value of molecular dipole moment $\boldsymbol{\mu}$ presented in Table 2 results from averaging this variable over all the molecules in the system and over the entire trajectory. This property fluctuates due to the flexible nature of most of the molecular models under consideration. Within condensed phases, in addition to flexibility,

For Peer Review Only

Table 1. Summary of thermodynamic properties (density ρ, thermal expansion coefficient α_P, isothermal compressibility κ_T, constant pressure heat capacity c_P, heat of vaporization ΔH_{vap}). Simulations are run at 298 K and 1 bar, except for the case of MEA for which the temperature is 293 K

	ρ (kg/m^3)	$10^3\ \alpha_P$ (K^{-1})	κ_T (GPa^{-1})	c_P (J mol^{-1} K^{-1})	ΔH_{vap} (kJ mol^{-1})
Water					
SPC	978.93 ± 0.02	0.733 ± 0.002	0.529 ± 0.002	83.6 ± 0.1	44.168 ± 0.001
TIP4P	998.88 ± 0.04	0.552 ± 0.003	0.512 ± 0.001	87.9 ± 0.1	43.920 ± 0.001
SPC/E	1000.14 ± 0.03	0.506 ± 0.004	0.459 ± 0.001	87.1 ± 0.2	49.239 ± 0.001
F-SPC	995.01 ± 0.02	0.528 ± 0.006	0.457 ± 0.001	112.0 ± 0.2	51.710 ± 0.001
Fw-SPC	1009.70 ± 0.04	0.459 ± 0.006	0.431 ± 0.002	114.1 ± 0.4	46.252 ± 0.002
Experiment	997.1 [59]	0.256 [60]	0.4525 [61]	75.29 [62]	43.87 [63]
Ethanol					
TraPPE-UA	782.4 ± 0.2	1.149 ± 0.006	1.263 ± 0.006	114.4 ± 0.4	46.891 ± 0.004
OPLS	793.21 ± 0.06	1.419 ± 0.004	1.002 ± 0.005	219.0 ± 0.4	45.455 ± 0.003
GAFF	794.16 ± 0.05	1.272 ± 0.005	0.976 ± 0.007	211.7 ± 0.4	47.514 ± 0.003
Experiment	784.8 [64]	1.09 [64]	1.15 [64]	112 [64]	42.32 [64]
Ethylene glycol					
TraPPE-UA	1129.78 ± 0.05	0.62 ± 0.02	0.411 ± 0.002	199 ± 3	80.862 ± 0.007
OPLS	1075.77 ± 0.05	0.80 ± 0.02	0.386 ± 0.003	261 ± 2	69.664 ± 0.005
GAFF	1176.52 ± 0.07	0.709 ± 0.008	0.241 ± 0.002	263.8 ± 0.3	83.911 ± 0.008
Experiment	1113.1 [65]	0.631 [66]	0.3686 [67] [a]	148.3425 ± 1.48467 [68]	65.99 ± 0.25 [69]
Propylene glycol					
TraPPE-UA	1042.0 ± 0.2	0.70 ± 0.02	0.591 ± 0.003	238 ± 5	78.85 ± 0.03
OPLS	1097.5 ± 0.2	0.98 ± 0.04	0.390 ± 0.007	334 ± 4	84.69 ± 0.02
GAFF	1120.06 ± 0.04	0.92 ± 0.03	0.307 ± 0.005	344 ± 4	82.318 ± 0.009
Experiment	1032.79 [70]	0.714 [71] [b]	—	190.54 ± 3.81 [72]	64.47 ± 0.18 [69]
Glycerol					
OPLS	1251.7 ± 0.2	0.80 ± 0.02	0.273 ± 0.004	361 ± 4	97.57 ± 0.03
GAFF	1302.9 ± 0.4	0.49 ± 0.02	0.166 ± 0.006	332 ± 8	102.57 ± 0.07
Experiment	1257.98 [73]	0.46 [74] [c]	0.24 [47] [c]	218.9 ± 0.2 [75]	91.7 ± 0.9 [75]
Monoethanolamine					
MEAa	1053.56 ± 0.02	1.01 ± 0.02	0.356 ± 0.002	376 ± 2	54.140 ± 0.004
OPLS	1024.12 ± 0.06	1.061 ± 0.006	0.457 ± 0.002	280.9 ± 0.6	59.222 ± 0.002
GAFF	1130.6 ± 0.1	0.75 ± 0.02	0.234 ± 0.003	289 ± 3	85.765 ± 0.008
Experiment	1018.0 [76]	0.801 ± 0.016 [77]	0.378 ± 0.038 [77]	144 [78]	64.03 [79]

[a] at 320K,

[b] at 0.8bar,

[c] at 293.15K

polarization effects have a significant effect on the molecular dipole moment, as compared to the gas phase [80]. However, polarizable force fields would be required if one wanted to obtain more accurate values of the liquid phase dipole moment. The relaxation time τ_D is obtained from an exponential fit of the long-time behavior of the dipole moment autocorrelation function, as explained in Sec. 2.3.

The first conclusion one can deduce from the results is that the prediction of dynamic and dielectric properties is generally not as good as that observed for the thermodynamic properties. This is expected, as the force fields used in this work were developed with the aim of reproducing the latter, and no dynamic properties were involved in their calibration.

3.2.2 Dynamic response: the dipole moment autocorrelation function

The dynamics of a molecular system can be analysed in terms of its dipole moment autocorrelation function. The relaxation times corresponding to the rotational and translational modes of a molecule or group of atoms within a larger molecule can be determined from the analysis of the time evolution of the dipole moment. The influence of an external electric field on these processes is believed to be the basis for the microwave heating mechanism. Figure 2 shows the Fourier transform of the dipole moment autocorrelation function $\hat{\phi}(\omega)$ for the different water models under consideration. The experimental data shown in this figure have been obtained using Eq. (12) to calculate the real and imaginary parts of $\hat{\phi}(\omega)$ from the experimental dielec-

For Peer Review Only

Table 2. Summary of dynamic properties (self-diffusion coefficient D, mean molecular dipole moment $\boldsymbol{\mu}$, static dielectric constant ε_0, relaxation time τ_D). Simulations are run at 298 K and 1 bar, except for the case of MEA for which the temperature is set to 293 K. * Experimental relaxation times τ_D are obtained fitting the experimental data in Figure 4 to the Debye model.

	10^9 D (10^{-9} m^2/s)	$\boldsymbol{\mu}$ (D^2)	ε_0	τ_D (ps)
Water				
SPC	3.96 ± 0.04	2.2740	66.6 ± 0.4	6.7 ± 0.2
TIP4P	3.65 ± 0.04	2.1775	44.5 ± 0.3	5.8 ± 0.2
SPC/E	2.50 ± 0.05	2.3506	70.6 ± 0.6	10.8 ± 0.2
F-SPC	2.64 ± 0.02	2.4580 ± 0.0001	94 ± 1	13.4 ± 0.4
Fw-SPC	2.12 ± 0.03	2.3949 ± 0.0001	80.2 ± 0.8	13.7 ± 0.2
Experiment	2.2999 ± 0.2300 [81]	2.9 ± 0.6 [82]	78.54 [83]	8.22*
Ethanol				
TraPPE-UA	1.15 ± 0.01	2.2625 ± 0.0001	18.1 ± 0.5	136 ± 6
OPLS	1.26 ± 0.03	2.3746 ± 0.0001	17.9 ± 0.3	53 ± 3
GAFF	1.04 ± 0.04	2.1234 ± 0.0002	15.6 ± 0.4	87 ± 3
Experiment	1.07 ± 0.11 [84]	3.43 [85]	25 [76]	187*
Ethylene glycol				
TraPPE-UA	0.0177 ± 0.0009	3.43 ± 0.02	36 ± 2	1000 ± 90
OPLS	0.141 ± 0.003	2.482 ± 0.005	20.3 ± 0.2	58 ± 2
GAFF	0.0146 ± 0.0008	3.209 ± 0.007	35.6 ± 0.5	430 ± 20
Experiment	—	4.02 [85]	40.86 [86]	123*
Propylene glycol				
TraPPE-UA	0.0212 ± 0.0006	3.28 ± 0.02	22.8 ± 0.9	1360 ± 70
OPLS	0.0135 ± 0.0009	4.04 ± 0.02	46 ± 3	2500 ± 300
GAFF	0.0129 ± 0.0005	3.13 ± 0.02	25.1 ± 0.6	600 ± 40
Experiment	0.0051 [87]	3.60 [88]	28.373 ± 0.004 [89]	342*
Glycerol				
OPLS	0.0030 ± 0.0003	4.453 ± 0.003	33 ± 3	2800 ± 300
GAFF	0.00068 ± 0.00003	3.45 ± 0.03	28 ± 5	9200 ± 900
Experiment	0.014 ± 0.004 [90]	4.21 [85]	42.54 [91]	933*
Monoethanolamine				
MEAa	0.181 ± 0.003	1.994 ± 0.004	10.5 ± 0.2	37.0 ± 0.6
OPLS	0.226 ± 0.004	3.462 ± 0.008	50.7 ± 0.9	87 ± 3
GAFF	0.0048 ± 0.0002	3.002 ± 0.004	40.9 ± 0.9	1320 ± 40
Experiment	0.054 ± 0.003 [92]	2.60 [88]	34.20 [93]	162*

tric spectrum of water, shown later in Fig. 4. In the case of water, it is clear that the flexible models and the SPC/E model overestimate both $\hat{\phi}'(\omega)$ and $\hat{\phi}''(\omega)$ in the microwave region, while SPC and TIP4P models underpredict the response. At higher frequencies, the characteristics of the different models seem to have less influence on the frequency dependence of the dynamic response. The rigid models clearly outperform the flexible ones, with the SPC model showing the best performance. According to the Debye model, the real and imaginary part of the Fourier transform of the dipole moment autocorrelation function are given by:

$$\phi'(\omega) = \frac{\tau_D}{1+\omega^2\tau_D^2}$$
$$\phi''(\omega) = \frac{\omega\tau_D^2}{1+\omega^2\tau_D^2} \qquad (15)$$

This shows how the frequency response of a molecular system is purely dependent on the relaxation time τ_D in the range of frequencies in which the Debye model is applicable. Figure 2 and the values of τ_D in Table 2 confirm the trends predicted by Eq. (15) in the case of water, which is a system known to be described accurately by the Debye model. The results for the remaining compounds are shown in the appendix. Analysing the different systems with respect to their frequency response, TraPPE-UA and GAFF force fields seem to provide slower dynamics than OPLS. This tendency is only reversed for propylene glycol. In the case of monoethanolamine,

For Peer Review Only

the MEAa force field predicts even faster dynamics than OPLS. This is mainly manifested by the positions of low frequency phenomena such as the decay in $\phi'(\omega)$ and the corresponding peak in $\phi''(\omega)$.

Once the dynamic response of the different systems has been obtained through the dipole moment autocorrelation function, the dielectric response is achieved through Eq. (12). To obtain an accurate description of dielectric spectra it becomes essential to have a good estimate of the static dielectric constant ε_0. The importance of the selection of this parameter is discussed in the following sections.

3.2.3 The static dielectric constant

The static dielectric constant is calculated using Neumann's formula [22, 58] that relates the static dielectric constant to the fluctuations of the total dipole moment of the system:

$$\varepsilon_0 = \varepsilon_\infty + \frac{4\pi}{3k_BTV}(\langle \mathbf{M}\cdot\mathbf{M}\rangle - \langle \mathbf{M}\rangle\cdot\langle \mathbf{M}\rangle) \tag{16}$$

where $k_B = 1.3806503\times10^{-23}\,\mathrm{m^2\,kg\,s^{-2}\,K^{-1}}$ is the Boltzmann constant, T is the temperature and V is the volume of the system.

The prediction of the static dielectric constant is poor in most cases (see Table 2), as none of the force fields examined here gives predictions that statistically agree with the experimental values. In the case of water, it would appear flexibility provides an improvement in the prediction of ε_0, particularly in the case of the Fw-SPC model, but this is at the cost of affecting the response at intermediate frequencies, as shown in Sec. 3.2.2.

The long correlation times in the fluctuations of total dipole moment make the calculation of the static dielectric constant difficult. Previous work has shown the importance of selecting the appropriate block length for the correct calculation of this property of water [94, 95]. This is confirmed by the results shown in Fig. 3 for the compounds studied in this work. To ensure the convergence of the static dielectric constant, the simulations are extended until the term containing the square of the average dipole moment $\left(\langle \mathbf{M}\rangle\cdot\langle \mathbf{M}\rangle\right)$ in Eq. (16) converges to zero, with a maximum simulation length of 100 ns. In this manner, we obtain converged values of the static dielectric constant for most models. However, this is clearly not valid in the case of glycerol for which longer simulations would be required to obtain the final value predicted by the models. Even ruling out the effect of the simulation length, most potential models do not seem to reach an acceptable agreement with the expected experimental value. It has been reported previously that this property is not well predicted by nonpolarizable force fields, such as the ones used in this work [47].

The consequence of this, through Eq. (12) and as shown in the next section, is that the loss factor is also poorly estimated, which in turn would lead to inaccurate estimates of dielectric heating rates. Therefore, due to the uncertainty in the prediction of the static dielectric constant, in Sec. 3.3 it is decided to use the corresponding experimental value in the determination of the dielectric spectra of the different systems under consideration. The effect of this choice on the shape of the dielectric spectra is also discussed in that section.

3.3 *Dielectric spectra*

3.3.1 Effect of the static dielectric constant on the dielectric spectrum

Figure 4 summarizes the results obtained in the prediction of the dielectric spectra of several organic compounds, applying the methodology explained in section 2.3. For the different molecules under consideration, dashed lines represent the best dielectric spectra predictions obtained using Eq. (12), when the static dielectric constant ε_0 is calculated from simulation data, using Neumann's approach (Eq. (16)). In most cases, the low-frequency end of the real part of the dielectric spectrum and the magnitude of the main absorption peak in the dielectric loss

For Peer Review Only

do not match the experimental result. Slight differences can be observed in the cases of water, propylene glycol and glycerol, while the results are clearly underestimated for ethanol and ethylene glycol, and overpredicted for MEA. This is related to the value of the static dielectric constant estimated by the different models (see Table 2). This variable acts as a scaling factor for the magnitude of both real and imaginary parts of the dielectric response. However, the dynamics (i.e. the frequency-dependence of $\varepsilon'(\omega)$ and $\varepsilon''(\omega)$) are not clearly affected by this fact and follow the experimental trend.

By using the experimental value of the static dielectric constant in Eq. (12), instead of the one obtained from the simulations, the dielectric spectra predictions are clearly improved (solid lines in Figure 4). Generally, a fairly good agreement with experimental data is reached, with at least one of the models providing an acceptable result. This demonstrates the importance of using a good value for the static dielectric constant. Even though the models may not reproduce the static dielectric constant, they do appear to correctly describe the dipole-dipole autocorrelation function $\phi(t)$. By simply introducing the experimental static dielectric constant in Eq. (12), one can obtain good results in the prediction of dielectric spectra. This is clearly the case for the models showing a better performance in the estimation of the dielectric spectra of ethanol (TraPPE-UA), ethylene glycol (OPLS) and MEA (OPLS), as shown in Figure 4. In the cases of propylene glycol (GAFF) and glycerol (OPLS), the improvement is also visible, although not so significant. Finally, the performance of the rigid SPC and TIP4P water models is significantly improved with respect to results obtained by English *et al.* [20, 21]. Therefore, one should not use the static dielectric constant as the only judge of the quality of a molecular model.

Although we recognize the theoretical inconsistency of substituting the calculated ε_0 by the experimental one, we consider this is a useful and practical method to estimate $\varepsilon'(\omega)$ and $\varepsilon''(\omega)$. It avoids the need for extraordinarily long simulations or highly accurate models to determine the static dielectric constant. This becomes particularly important when a good knowledge of the magnitude of the dielectric response is required for the prediction of the heat a molecular system can absorb from a microwave field (see Eq. (3)). It seems unlikely that classical force fields of the type used here will ever be satisfactory for production of a wide range of thermodynamic and dynamical phenomena simultaneously, and so methods that can correct for their weaknesses are desirable. In this case, we have shown that prediction of dielectric heating can be systematically improved if the experimental static dielectric constant is known a priori.

3.3.2 Deviations from the Debye model

The main absorption peak observed in the low frequency end of the imaginary part of the dielectric spectrum (see Figure 4) is associated with dipole reorientation as a response to a time-dependent electric field [7, 96, 97]. It is typically known as α-relaxation peak, and for relatively small molecules such as the ones studied here, it usually occurs in the microwave or high frequency radio wave region at ambient conditions.

As a description of this process, the Debye model (see Eq. (2)) assumes dipoles relax independently from each other with a common relaxation time. However, in most materials this somehow 'ideal' behaviour does not take place. Cole and Davidson [4] suggested an empirical expression for the complex frequency-dependent permittivity which takes into account deviations from the Debye relaxation model:

$$\hat{\varepsilon}(\omega) = \varepsilon_\infty + \frac{\varepsilon_0 - \varepsilon_\infty}{[1 + i\,\omega\tau_{CD}]^\beta} \tag{17}$$

where τ_{CD} is the characteristic relaxation time, and β accounts for the symmetric broadness and asymmetry in the resulting dielectric spectra, respectively. In Fig. 4 we include the fits of the α-relaxation peak in the imaginary part of the dielectric permittivity to both the Debye and the Cole-Davidson models, for the force fields that show the best performance in the prediction of the dielectric spectrum of each of the compounds. The former uses the values of τ_D shown in Table 2, while for the latter, the fitting parameters τ_{CD} and β are presented in Table 3. These

For Peer Review Only

Table 3. Cole-Davidson fit parameters.

	τ_{CD} / ps	β		τ_{CD} / ps	β
Water			**Propylene glycol**		
SPC	7.2 ± 0.2	0.91 ± 0.01	TraPPE-UA	1830 ± 70	0.71 ± 0.02
TIP4P	6.40 ± 0.07	0.895 ± 0.009	OPLS	3100 ± 500	0.77 ± 0.03
SPC/E	11.6 ± 0.2	0.927 ± 0.002	GAFF	810 ± 50	0.71 ± 0.02
F-SPC	14.3 ± 0.4	0.935 ± 0.006			
Fw-SPC	14.8 ± 0.3	0.92 ± 0.01			
Ethanol			**Glycerol**		
TraPPE-UA	173 ± 7	0.766 ± 0.0.05			
OPLS	75 ± 4	0.67 ± 0.01	OPLS	3700 ± 300	0.72 ± 0.03
GAFF	111 ± 4	0.759 ± 0.002	GAFF	13000 ± 1000	0.74 ± 0.04
Ethylene glycol			**Monoethanolamine**		
TraPPE-UA	1300 ± 200	0.74 ± 0.03	MEAa	53 ± 2	0.65 ± 0.02
OPLS	71 ± 2	0.793 ± 0.008	OPLS	97 ± 3	0.891 ± 0.004
GAFF	550 ± 30	0.75 ± 0.02	GAFF	1750 ± 70	0.72 ± 0.02

are obtained by fitting the simulation results to the Cole-Davidson equation using the method of least squares. With the goal of making the fitting procedure more uniform, the fit is performed on the data above half height of the main absorption peak. As β approaches unity, Cole and Davidson's model reduces to the Debye model. As deduced from both Fig. 4 and the value of the parameters of the Cole-Davidson model, water is the system that conforms most closely to the Debye model. The deviation of β from unity results in an asymmetric broadening of the spectrum or excess wing [97]. This means that the relaxation time predicted by this model will no longer coincide with the relaxation time corresponding to the maximum loss as estimated by the Debye model. This is clearly the case for ethanol OPLS, where τ_{CD} is definitely larger than τ_D. For other systems, the more β differs from one, the larger is the relaxation time predicted by the Cole-Davidson model with respect to Debye relaxation time.

3.3.3 Effect of size and polarity

Finally, the dielectric spectra of the different substances under consideration are compared in Fig. 5, using the results provided by the best force fields in every case. This clearly shows how as the size of the molecule increases the relaxation frequency decreases (i.e. the dynamics slow down). In addition, it is possible to observe the effect of polarity on the maximum of the dielectric loss (i.e. the more polar species show a higher peak and, consequently, have the higher potential to transform electromagnetic energy into heat).

4 Conclusions

In this work, we have examined the ability of molecular dynamics simulations to predict the dielectric spectra of small molecules in the microwave region. This is an essential feature if one wants to estimate the heat a dielectric material can absorb from an external microwave field. The methodology used here analyses the time fluctuations of the total dipole moment of a molecular system. All-atom and united-atom force fields, which have mainly been developed to accurately reproduce experimental thermodynamic properties, generally give good predictions for the frequency-dependent dielectric constant of a series of alcohols and glycols, as well as for monoethanolamine, so long as the correct value of the static dielectric constant is used.

Despite the good performance in describing the dynamics of the dielectric response of the systems under consideration, most of the models have difficulties in predicting the static dielectric constant, which is a crucial parameter in the scaling of dielectric spectra. The use of non-polarizable force fields in our simulations may have an influence on the molecular motion, hence affecting the static dielectric constant. Another limiting factor could be the long time scales required to achieve an accurate value of this property, which corresponds to the magnitude of total dipole moment fluctuations, especially for larger systems.

For Peer Review Only

The solution adopted here is to use the experimental value of this magnitude in conjunction with the dynamics predicted by molecular simulations. This can avoid the need for extraordinarily long simulations for systems for which the static dielectric constant is a well known property or can be easily measured experimentally.

With these considerations in mind, the models evaluated in this work are able to capture the main experimental features. The simulated dielectric spectra of all the systems we analyse exhibit an α-relaxation peak, characteristic of these types of substances. In addition, while water possesses a Debye-like relaxation, alcohols, glycols and monoethanolamine show signs of an excess wing in the high frequency end of the α-relaxation peak, which has been described in the literature [97]

Currently, due to limitations in computational hardware, all-atom molecular dynamics simulations cannot describe interesting features in the dielectric relaxation of a material that occur on times scales greater than or on the order of μs. However, the ability of these simulations to reproduce the characteristics of the dielectric spectra at higher frequencies, as demonstrated here, gives confidence on the possibility of using the force fields studied in this work for the prediction of dielectric spectra of compounds for which experimental data are not available. Together with other recent work in this field, this study opens the possibility to use molecular dynamics simulations as a powerful tool in areas such as the study of glass-forming materials, the analysis of polymer dynamics or the examination of the dielectric behaviour of mixtures.

Acknowledgments

The authors gratefully acknowledge the support of the Department of Chemical and Process Engineering at the University of Strathclyde and the School of Engineering at the University of Edinburgh, as well as the Engineering and Physical Sciences Research Council (EPSRC). Results were obtained using the EPSRC funded ARCHIE-WeSt High Performance Computer (www.archie-west.ac.uk). EPSRC grant no. EP/K000586/1.

References

[1] R. Cherbanski and E. Molga, *Intensification of desorption processes by use of microwaves - An overview of possible applications and industrial perspectives*, Chem. Eng. Process: Process Intensification 48 (2009), pp. 48 – 58.
[2] A.M. Holtzer, *The collected papers of Peter J. W. Debye*, J. Polym. Sci. 13 (1954), pp. 548–548.
[3] K.S. Cole and R.H. Cole, *Dispersion and Absorption in Dielectrics I. Alternating Current Characteristics*, J. Chem. Phys. 9 (1941), pp. 341–351.
[4] D.W. Davidson and R.H. Cole, *Dielectric Relaxation in Glycerine*, J. Chem. Phys. 18 (1950), pp. 1417–1417.
[5] S. Havriliak and S. Negami, *A complex plane representation of dielectric and mechanical relaxation processes in some polymers*, Polymer 8 (1967), pp. 161 – 210.
[6] A. Hozde la and A. Loupy (eds.), 3 ed., Wiley-VCH, 2012.
[7] F. Kremer and A. Schonhals (eds.), Springer, 2002.
[8] W.J. Ellison, *Permittivity of Pure Water, at Standard Atmospheric Pressure, over the Frequency Range 0-25THz and the Temperature Range 0-100C*, Journal of Physical and Chemical Reference Data 36 (2007), pp. 1–18.
[9] U. Kaatze and V. Uhlendorf, *The Dielectric Properties of Water at Microwave Frequencies*, Z. Phys. Chem. Neue Fol. 126 (1981), pp. 151–165.
[10] U. Kaatze, *Complex permittivity of water as a function of frequency and temperature*, J. Chem. Eng. Data 34 (1989), pp. 371–374.
[11] J. Barthel, K. Bachhuber, R. Buchner, and H. Hetzenauer, *Dielectric spectra of some common solvents in the microwave region. Water and lower alcohols*, Chem. Phys. Lett. 165 (1990), pp. 369 – 373.
[12] J.B. Hasted and S.H.M. El Sabeh, *The dielectric properties of water in solutions*, Trans. Faraday Soc. 49 (1953), pp. 1003–1011.
[13] D.W. Davidson and R.H. Cole, *Dielectric Relaxation in Glycerol, Propylene Glycol, and n-Propanol*, J. Chem. Phys. 19 (1951), pp. 1484–1490.
[14] R.H. Cole and D.W. Davidson, *High Frequency Dispersion in n-Propanol*, J. Chem. Phys. 20 (1952), pp. 1389–1391.
[15] J. Poley, *Microwave dispersion of some polar liquids*, Technische Hogeschool te Delft, 1955.
[16] R.W. Rampolla, R.C. Miller, and C.P. Smyth, *Microwave Absorption and Molecular Structure in Liquids. XXV. Measurements of Dielectric Constant and Loss at 3.1-mm Wavelength by an Interferometric Method*, J. Chem. Phys. 30 (1959), pp. 566–573.
[17] J.A. Saxton, R.A. Bond, G.T. Coats, and R.M. Dickinson, *Dispersion at Millimeter Wavelengths in Methyl and Ethyl Alcohols*, J. Chem. Phys. 37 (1962), pp. 2132–2138.

For Peer Review Only

[18] D.E. Buck, *The dielectric spectra of ethanol-water mixtures in the microwave region*, Massachusetts Institute of Technology. Dept. of Chemistry., 1965.
[19] S.W. Rick, S.J. Stuart, and B.J. Berne, *Dynamical fluctuating charge force fields: Application to liquid water*, J. Chem. Phys. 101 (1994), pp. 6141–6156.
[20] N.J. English and J.M.D. MacElroy, *Atomistic simulations of liquid water using Lekner electrostatics*, Mol. Phys. 100 (2002), pp. 3753–3769.
[21] N.J. English, *Molecular dynamics simulations of liquid water using various long-range electrostatics techniques*, Mol. Phys. 103 (2005), pp. 1945–1960.
[22] M. Neumann and O. Steinhauser, *On the calculation of the frequency-dependent dielectric constant in computer simulations*, Chem. Phys. Lett. 102 (1983), pp. 508 – 513.
[23] M. Neumann and O. Steinhauser, *Computer simulation and the dielectric constant of polarizable polar systems*, Chem. Phys. Lett. 106 (1984), pp. 563 – 569.
[24] N.J. English and J.M.D. MacElroy, *Molecular dynamics simulations of microwave heating of water*, J. Chem. Phys. 118 (2003), pp. 1589–1592.
[25] N.J. English and J.M.D. MacElroy, *Hydrogen bonding and molecular mobility in liquid water in external electromagnetic fields*, J. Chem. Phys. 119 (2003), pp. 11806–11813.
[26] N.J. English, *Molecular dynamics simulations of microwave effects on water using different long-range electrostatics methodologies*, Mol. Phys. 104 (2006), pp. 243–253.
[27] J. Petravic and J. Delhommelle, *Conductivity of molten sodium chloride in an alternating electric field*, J. Chem. Phys. 119 (2003), pp. 8511–8518.
[28] N.J. English, D.C. Sorescu, and J.K. Johnson, *Effects of an external electromagnetic field on rutile Tio2: A molecular dynamics study*, J. Phys. Chem. Solids 67 (2006), pp. 1399 – 1409.
[29] C. Desgranges and J. Delhommelle, *Estimating the conductivity of a nanoconfined liquid subjected to an experimentally accessible external field*, Mol. Simulat. 34 (2008), pp. 177–181.
[30] N.J. English and D.A. Mooney, *Very Different Responses to Electromagnetic Fields in Binary Ionic Liquid-Water Solutions*, J. Phys. Chem. B 113 (2009), pp. 10128–10134.
[31] N.J. English and D.A. Mooney, *Electromagnetic field effects on binary dimethylimidazolium-based ionic liquid/water solutions*, Phys. Chem. Chem. Phys. 11 (2009), pp. 9370–9374.
[32] N.J. English, D.A. Mooney, and S.W. O'Brien, *Electrical conductivity and dipolar relaxation of binary dimethylimidazolium chloride-water solutions: A molecular dynamics study*, J. Mol. Liq. 157 (2010), pp. 163 – 167.
[33] N.J. English, D.A. Mooney, and S. O'Brien, *Ionic liquids in external electric and electromagnetic fields: a molecular dynamics study*, Mol. Phys. 109 (2011), pp. 625–638.
[34] D.V. Matyushov, *On the theory of dielectric spectroscopy of protein solutions*, Journal of Physics: Condensed Matter 24 (2012), p. 325105.
[35] M. Heyden, D.J. Tobias, and D.V. Matyushov, *Terahertz absorption of dilute aqueous solutions*, The Journal of Chemical Physics 137 (2012), 235103, pp. –.
[36] D.R. Martin and D.V. Matyushov, *Hydration shells of proteins probed by depolarized light scattering and dielectric spectroscopy: Orientational structure is significant, positional structure is not*, The Journal of Chemical Physics 141 (2014), 22D501, pp. –.
[37] M.B. Sweatman, *Equilibrium behaviour of a novel gas separation process, with application to carbon capture*, Chem. Eng. Sci. 65 (2010), pp. 3907 – 3913.
[38] M.B. Sweatman, *Improving the equilibrium performance of active carbons for separation processes by co-adsorption with low pressure solvent: application to carbon capture*, Adsorption 17 (2011), pp. 723–737.
[39] H.J.C. Berendsen, J.P.M. Postma, W.F. Gunsterenvan , and J. Hermans D. Reidel Publishing Company, 1981, pp. 331–342.
[40] W.L. Jorgensen, J. Chandrasekhar, J.D. Madura, R.W. Impey, and M.L. Klein, *Comparison of simple potential functions for simulating liquid water*, J. Chem. Phys. 79 (1983), pp. 926–935.
[41] H.J.C. Berendsen, J.R. Grigera, and T.P. Straatsma, *The missing term in effective pair potentials*, The Journal of Physical Chemistry 91 (1987), pp. 6269–6271.
[42] D.M. Ferguson, *Parameterization and evaluation of a flexible water model*, J. Comput. Chem. 16 (1995), pp. 501–511.
[43] Y. Wu, H.L. Tepper, and G.A. Voth, *Flexible simple point-charge water model with improved liquid-state properties*, J. Chem. Phys. 124 (2006), 024503, p. 024503.
[44] B. Chen, J.J. Potoff, and J.I. Siepmann, *Monte Carlo Calculations for Alcohols and Their Mixtures with Alkanes. Transferable Potentials for Phase Equilibria. 5. United-Atom Description of Primary, Secondary, and Tertiary Alcohols*, J. Phys. Chem. B 105 (2001), pp. 3093–3104.
[45] J.M. Stubbs, J.J. Potoff, and J.I. Siepmann, *Transferable Potentials for Phase Equilibria. 6. United-Atom Description for Ethers, Glycols, Ketones, and Aldehydes*, J. Phys. Chem. B 108 (2004), pp. 17596–17605.
[46] W.L. Jorgensen and J. Tirado-Rives, *Potential energy functions for atomic-level simulations of water and organic and biomolecular systems*, P. Natl. Acad. Sci. USA 102 (2005), pp. 6665–6670.
[47] C. Caleman, P.J. Maarenvan , M. Hong, J.S. Hub, L.T. Costa, and D. Spoelvan der , *Force Field Benchmark of Organic Liquids: Density, Enthalpy of Vaporization, Heat Capacities, Surface Tension, Isothermal Compressibility, Volumetric Expansion Coefficient, and Dielectric Constant*, J. Chem. Theory Comput. 8 (2012), pp. 61–74.
[48] J. Wang, R.M. Wolf, J.W. Caldwell, P.A. Kollman, and D.A. Case, *Development and testing of a general amber force field*, J. Comput. Chem. 25 (2004), pp. 1157–1174.
[49] E.F. Silvada , T. Kuznetsova, B. Kvamme, and K.M. Merz, *Molecular Dynamics Study of Ethanolamine as a Pure Liquid and in Aqueous Solution*, J. Phys. Chem. B 111 (2007), pp. 3695–3703.
[50] B. Hess, C. Kutzner, D. Spoelvan der , and E. Lindahl, *GROMACS 4: Algorithms for Highly Efficient, Load-Balanced, and Scalable Molecular Simulation*, J. Chem. Theory Comput. 4 (2008), pp. 435–447.
[51] R. Hockney, S. Goel, and J. Eastwood, *Quiet high-resolution computer models of a plasma*, J. Comput. Phys. 14 (1974), pp. 148 – 158.
[52] S. Nose, *A molecular dynamics method for simulations in the canonical ensemble*, Mol. Phys. 52 (1984), pp. 255–268.
[53] W.G. Hoover, *Canonical dynamics: Equilibrium phase-space distributions*, Phys. Rev. A 31 (1985), pp. 1695–1697.
[54] M. Parrinello and A. Rahman, *Polymorphic transitions in single crystals: A new molecular dynamics method*, J. Appl. Phys. 52 (1981), pp. 7182–7190.
[55] S. Nos and M. Klein, *Constant pressure molecular dynamics for molecular systems*, Mol. Phys. 50 (1983), pp. 1055–

For Peer Review Only

1076.
[56] B. Hess, H. Bekker, H.J.C. Berendsen, and J.G.E.M. Fraaije, *LINCS: A linear constraint solver for molecular simulations*, J. Comput. Chem. 18 (1997), pp. 1463–1472.
[57] T. Darden, D. York, and L. Pedersen, *Particle mesh Ewald: An N [center-dot] log(N) method for Ewald sums in large systems*, J. Chem. Phys. 98 (1993), pp. 10089–10092.
[58] M.P. Allen and D.J. Tildesley Clarendon Press, New York, NY, USA, 1989.
[59] X. Zhang and C. Jian, *Liquid-Liquid Equilibrium for the Ternary System Methanol + Acrylonitrile + Water*, J. Chem. Eng. Data 57 (2012), pp. 142–147.
[60] Z. Orekhova, M. Ben-Hamo, E. Manzurola, and A. Apelblat, *Electrical Conductance and Volumetric Studies in Aqueous Solutions of Nicotinic Acid*, J. Solution Chem. 34 (2005), pp. 687–700.
[61] H. Doi, K. Tamura, and S. Murakami, *Thermodynamic properties of aqueous solution of 2-isobutoxyethanol at T = (293.15, 298.15, and 303.15) K, below and above LCST*, J. Chem. Thermodyn. 32 (2000), pp. 729 – 741.
[62] A.M. Kolker and L.P. Safonova, *Molar heat capacities of the (water + acetonitrile) mixtures at T = (283.15, 298.15, 313.15, and 328.15) K*, J. Chem. Thermodyn. 42 (2010), pp. 1209 – 1212.
[63] M. Antosik, M. Galka, and S.K. Malanowski, *Vapor-Liquid Equilibrium in a Ternary System Cyclohexane + Ethanol + Water*, J. Chem. Eng. Data 49 (2004), pp. 7–10.
[64] Y. Marcus Wiley, 1998, p. 254.
[65] S.K. Begum, R.J. Clarke, M.S. Ahmed, S. Begum, and M.A. Saleh, *Densities, Viscosities, and Surface Tensions of the System Water + Diethylene Glycol*, J. Chem. Eng. Data 56 (2011), pp. 303–306.
[66] D. Egorov G.I.and Makarov, *The bulk properties of ethylene glycol - dimethylsulfoxide mixtures over the temperture range 278-323 K at p = 0.1 MPa*, Zh. fiz. khim+ 82 (2008), pp. 1982–1988.
[67] M.G. Technische Hochschule Carl Schorlemmer Leuna-Merseburg, *Unpublished data*; 1989 Unpublished data.
[68] C. Yang, P. Ma, F. Jing, and D. Tang, *Excess Molar Volumes, Viscosities, and Heat Capacities for the Mixtures of Ethylene Glycol + Water from 273.15 K to 353.15 K*, J. Chem. Eng. Data 48 (2003), pp. 836–840.
[69] S.P. Verevkin, *Determination of vapor pressures and enthalpies of vaporization of 1,2-alkanediols*, Fluid Phase Equilibr. 224 (2004), pp. 23 – 29.
[70] M. Rodrigues and A. Francesconi, *Experimental Study of the Excess Molar Volumes of Binary and Ternary Mixtures Containing Water + (1,2-Ethanediol, or 1,2-Propanediol, or 1,3-Propanediol, or 1,2-Butanediol) + (1-n-Butyl-3-methylimidazolium Bromide) at 298.15 K and Atmospheric Pressure*, J. Sol. Chem. 40 (2011), pp. 1863–1873.
[71] H.A. Zarei, S. Asadi, and H. Iloukhani, *Temperature dependence of the volumetric properties of binary mixtures of (1-propanol, 2-propanol and 1,2-propanediol) at ambient pressure (81.5 kPa)*, J. Mol. Liq. 141 (2008), pp. 25 – 30.
[72] C. Yang, P. Ma, and S. Xia, *Heat capacity of glycol determined by differential scanning calorimeter*, Tianjin Daxue Xuebao 36 (2003), pp. 192–196.
[73] R. Belda Maximino, *Viscosity and density of binary mixtures of alcohols and polyols with three carbon atoms and water: equation for the correlation of viscosities of binary mixtures*, Phys. Chem. Liq. 47 (2009), pp. 515–529.
[74] C.L. Yaws McGraw-Hill, 2003.
[75] M. Bastos, S.O. Nilsson, M.D.R. Silvada , M.A.R. Silvada , and I. Wads, *Thermodynamic properties of glycerol enthalpies of combustion and vaporization and the heat capacity at 298.15 K. Enthalpies of solution in water at 288.15, 298.15, and 308.15 K*, J. Chem. Thermodyn. 20 (1988), pp. 1353 – 1359.
[76] D.R. Lide 90th ed., CRC Press, 2009.
[77] V. Kartsev, M. Rodnikova, V. Tsepulin, and V. Markova, *Piezometry and Densitometry of Aqueous Solutions of Diamines, Aminoalcohols, and Diols. II. Solutions of Monoethanolamine and Diols*, Russ. J. Phys. Chem. 62 (1988), pp. 1152–1153.
[78] G. Liessmann, W. Schmidt, and S. Reiffarth, Recommended Thermophysical Data; .
[79] DIPPR Design Institute for Physical Properties Research, AIChE, 2010.
[80] A.A. Chialvo, F. Moucka, L. Vlcek, and I. Nezbeda, *Vapor-Liquid Equilibrium and Polarization Behavior of the GCP Water Model: Gaussian Charge-on-Spring versus Dipole Self-Consistent Field Approaches to Induced Polarization*, The Journal of Physical Chemistry B 119 (2015), pp. 5010–5019 PMID: 25803267.
[81] M. Holz, S.R. Heil, and A. Sacco, *Temperature-dependent self-diffusion coefficients of water and six selected molecular liquids for calibration in accurate 1H NMR PFG measurements*, Phys. Chem. Chem. Phys. 2 (2000), pp. 4740–4742.
[82] Y.S. Badyal, M. Saboungi, D.L. Price, S.D. Shastri, D.R. Haeffner, and A.K. Soper, *Electron distribution in water*, The Journal of Chemical Physics 112 (2000), pp. 9206–9208.
[83] G. Gente and C. La Mesa, *Water-Trifluoroethanol Mixtures: Some Physicochemical Properties*, J. Solution Chem. 29 (2000), pp. 1159–1172.
[84] M. Holz, X.a. Mao, D. Seiferling, and A. Sacco, *Experimental study of dynamic isotope effects in molecular liquids: Detection of translation-rotation coupling*, J. Chem. Phys. 104 (1996), pp. 669–679.
[85] T. Hanai, N. Koizumi, and R. Gotoh, *Temperature Dependence of Dielectric Constants and Dipole Moments in Polar Liquids*, Bull. Inst. Chem. Res, Kyoto Univ. 39 (1961), pp. 195–201.
[86] C.M. Kinart and M. Klimczak, *Thermodynamic and structural properties of binary mixtures of some glycols with 2-butoxyethanol at T=293.15, 298.15 and 303.15 K*, J. Mol. Liq. 148 (2009), pp. 132 – 139.
[87] M. Mitchell and H.J.V. Tyrrell, *Diffusion of benzene, phenol and resorcinol in propane-1,2-diol, and the validity of the Stokes-Einstein equation*, J. Chem. Soc., Faraday Trans. 2 68 (1972), pp. 385–399.
[88] J. Gmehling, J. Krafczyk, J. Ahlers, S. Nebig, I. Hunecker, M. Eisel, D. Fischer, B. Krentscher, and K. Beyer, Pure compound data from DDB; .
[89] N.V. Sastry and M.C. Patel, *Densities, Excess Molar Volumes, Viscosities, Speeds of Sound, Excess Isentropic Compressibilities, and Relative Permittivities for Alkyl (Methyl, Ethyl, Butyl, and Isoamyl) Acetates + Glycols at Different Temperatures*, J. Chem. Eng. Data 48 (2003), pp. 1019–1027.
[90] G. D'Errico, O. Ortona, F. Capuano, and V. Vitagliano, *Diffusion Coefficients for the Binary System Glycerol + Water at 25 C. A Velocity Correlation Study*, J. Chem. Eng. Data 49 (2004), pp. 1665–1670.
[91] C.M. Kinart and W.J. Kinart, *Physicochemical Properties of Glycerol-Formamide Liquid Mixtures and Their Assumed Internal Structures*, Phys. Chem. Liq. 33 (1996), pp. 159–170.
[92] M. Rodnikova, V. Privalov, F. Samigullin, and V. Zhakova, *Rotational and progressive molecules mobility of certain aminoalcohols*, Zh. Fiz. Khim+ 68 (1994), pp. 2235–2238.
[93] P. Undre, S. Helambe, S. Jagdale, P. Khirade, and S. Mehrotra, *Study of solute-solvent interaction through dielectrics properties of N,N-dimethylacetamide in ethanolamine*, J. Mol. Liq. 137 (2008), pp. 147 – 151.

For Peer Review Only

[94] O. Gereben and L. Pusztai, *On the accurate calculation of the dielectric constant from molecular dynamics simulations: The case of SPC/E and SWM4-DP water*, Chem. Phys. Lett. 507 (2011), pp. 80 – 83.
[95] G. Raabe and R.J. Sadus, *Molecular dynamics simulation of the dielectric constant of water: The effect of bond flexibility*, J. Chem. Phys. 134 (2011), 234501, pp. –.
[96] U. Schneider, P. Lunkenheimer, R. Brand, and A. Loidl, *Dielectric and far-infrared spectroscopy of glycerol*, J. Non-Cryst. Solids 235-237 (1998), pp. 173 – 179.
[97] P. Lunkenheimer, U. Schneider, R. Brand, and A. Loid, *Glassy dynamics*, Contemp. Phys. 41 (2000), pp. 15–36.
[98] S. Horikoshi, S. Matsuzaki, T. Mitani, and N. Serpone, *Microwave frequency effects on dielectric properties of some common solvents and on microwave-assisted syntheses: 2-Allylphenol and the C12-C2-C12 Gemini surfactant*, Radiat. Phys. Chem. 81 (2012), pp. 1885 – 1895.
[99] M. Zahn, Y. Ohki, D.B. Fenneman, R. Gripshover, and J. Gehman V.H., *Dielectric properties of water and water/ethylene glycol mixtures for use in pulsed power system design*, Proc. IEEE 74 (1986), pp. 1182–1221.
[100] J. Bartos, O. Sausa, M. Kohler, H. Svajdlenkova, P. Lunkenheimer, J. Kristiak, and A. Loidl, *Positron annihilation and broadband dielectric spectroscopy: A series of propylene glycols*, J. Non-Cryst. Solids 357 (2011), pp. 376 – 384 6th International Discussion Meeting on Relaxation in Complex Systems.
[101] P. Lunkenheimer, A. Pimenov, B. Schiener, R. Bohmer, and A. Loidl, *High-frequency dielectric spectroscopy on glycerol*, Europhys. Lett. 33 (1996), p. 611.
[102] P. Lunkenheimer, A. Pimenov, M. Dressel, Y.G. Goncharov, R. Bohmer, and A. Loidl, *Fast Dynamics of Glass-Forming Glycerol Studied by Dielectric Spectroscopy*, Phys. Rev. Lett. 77 (1996), pp. 318–321.
[103] A. Patil and V. Pawar, *Microwave dielectric spectra and molecular interaction in a binary mixture of ethanolamine with diethanolamine*, J. Mol. Liq. 188 (2013), pp. 1 – 4.
[104] A. Patil, G. Shinde, and V. Pawar, *Dielectric relaxation study of hydrogen bonded structures in ethanolamine with diethanolamine using {TDR} technique*, J. Mol. Liq. 168 (2012), pp. 42 – 46.

For Peer Review Only

Figure 1. Molecular models used in this study. Carbon, Oxygen, Nitrogen and Hydrogen atoms are represented as grey, blue, green and white circles, respectively. The extra site in the TIP4P water model is shown as a light orange circle. Partial charges appear as dark green dots while Lennard-Jones interaction sites are represented as red dots.

Figure 2. Dynamics of water at 298 K and 1 bar through the Fourier transform of the dipole moment autocorrelation function. Blue, green, magenta, orange and red lines show the results corresponding to the SPC, TIP4P, SPC/E, F-SPC and Fw-SPC models, respectively. Black circles represent experimental values obtained from Eq. (12) using dielectric spectrum data from different sources [9–12].

Figure 3. Effect of the block length on the static dielectric constant. The results show running averages started from an energetically equilibrated sample. They are obtained via molecular dynamics simulations at 298 K and 1 bar, using Neumann's formula (Eq. 16). For MEA, the simulations are performed at 293 K. Solid lines represent the results obtained using the different force fields introduced in the text. Dashed lines correspond to the term containing the square of the average dipole moment $\left(\langle \mathbf{M} \rangle \cdot \langle \mathbf{M} \rangle\right)$ in Eq. 16, which should vanish at long times to consider the static dielectric constant converged. In the particular case of water, blue, green, magenta, orange and red lines show the results corresponding to the SPC, TIP4P, SPC/E, F-SPC and Fw-SPC models, respectively. For the remainder substances, red, green, blue and magenta lines represent results generated using the TraPPE-UA, OPLS, GAFF and MEAa force fields, respectively. Dotted horizontal lines represent experimental values obtained from different sources: water [83], ethanol [76], ethylene glycol [86], propylene glycol [89], glycerol [91] and MEA [93].

Figure 4. Dielectric response of several organic compounds obtained via molecular dynamics simulations at 298 K and 1 bar. For monoethanolamine (MEA), the simulations are performed at 293 K. Solid lines represent the results obtained in our simulations using the different force fields introduced in the text, and employing the experimental static dielectric constant in the calculations. In the particular case of water, blue, green, magenta, orange and red lines show the results corresponding to the SPC, TIP4P, SPC/E, F-SPC and Fw-SPC models, respectively. For the remaining substances, red, green, blue and magenta lines represent results generated using the TraPPE-UA, OPLS, GAFF and MEAa force fields, respectively. Dashed lines correspond to results using Neumann's formula (Eq. 16) to calculate the static dielectric constant, for the force fields showing a better performance in the prediction of the dielectric spectrum in every case (water SPC, ethanol TraPPE-UA, ethylene glycol OPLS, propylene glycol GAFF, glycerol OPLS and MEA OPLS). Black circles represent experimental values obtained from different sources for the following systems: water [9–12], ethanol [16–18, 98], ethylene glycol [99], propylene glycol [100], glycerol [96, 97, 101, 102]. For MEA, black open and filled circles are experimental values of the dielectric spectrum at 278 K [103] and 308 K [104] respectively. Black dot-dash and dotted lines in $\varepsilon''(\omega)$ represent the fit of the α-relaxation peak to Debye and Cole-Davidson models, respectively.

Figure 5. Comparison of the dielectric spectra of different organic substances. The force fields that show a better performance in the prediction of the dielectric response are used in this representation: water SPC (blue), ethanol TraPPE-UA (red), ethylene glycol OPLS (black), propylene glycol GAFF (orange), glycerol OPLS (green) and MEA OPLS (magenta).

For Peer Review Only

Appendix A: Force fields parameters

Water models:

- The simple point charge (SPC) model [39] is a rigid model in which the water molecule is formed by three Coulomb interaction sites centred on the atomic nuclei and one LJ interaction site situated on the oxygen atom. The SPC model is one of the more broadly used water models, and, despite its simplicity, it provides a good description of most properties of water.
- The TIP4P model [40] is a 4-site water model. Its main characteristic is that the partial negative charge of the oxygen atom is moved towards the hydrogen atoms at a point M situated along the bisector of the bond angle. As a result, the electrostatic distribution around the molecule is improved. The simple form of this model and its acceptable performance justify its wide implementation in computational chemistry.
- The SPC/E model [41] imposes a change in polarization with respect to the SPC model by modifying the charges on oxygen and hydrogen atoms. This results in a better prediction of density, as well as diffusion and dielectric constants.
- Based on the SPC model, the Flexible SPC (F-SPC) model [42] adds harmonic and anharmonic terms to describe bond stretching and angle bending. Inclusion of these terms has been shown to lead to improved predictions for thermodynamic, dielectric and dynamic properties.
- Another flexible model showing good results is the Fw-SPC water model [43] which is one of the most accurate non-polarizable models. Its development has shown how important bond stretching and angle bending are for the accurate determination of the self-diffusion coefficient and dielectric constant respectively.

Table A1. Parameters of water models

Model	SPC	TIP4P	SPC/E	F-SPC	Fw-SPC
σ_O (nm)	0.316557	0.315365	0.316557	0.318259	0.3165492
ϵ_O (kJ mol^{-1})	0.650194	0.648520	0.650194	0.629616	0.6496778
σ_H (nm)	0.000000	0.000000	0.000000	0.0000000	0.000000
ϵ_H (kJ mol^{-1})	0.000000	0.000000	0.000000	0.0000000	0.000000
σ_M (nm)	—	0.000000	—	—	—
ϵ_M (kJ mol^{-1})	—	0.000000	—	—	—
b_0 (nm)	0.10000	0.09572	0.10000	0.10000	0.1012
b_M (nm)	—	0.015	—	—	—
k_b (kJ mol^{-1} nm^{-2})	—	—	—	229074 [a]	442729.7
k_{cub} (nm^{-1})	—	—	—	−16.5 [a]	—
θ_0 (°)	109.47	104.52	109.47	109.5	113.24
k_a (kJ mol^{-1} rad^{-2})	—	—	—	417.6	317
q_O (e)	−0.82	—	−0.8476	−0.826	−0.82
q_H (e)	0.41	0.52	0.4238	0.413	0.41
q_M (e)	—	−1.04	—	—	—

[a]The F-SPC model uses a cubic bond stretching potential of the form: $U_b(r_{ij}) = k_b(r_{ij} - b_0)^2 + k_b k_{cub}(r_{ij} - b_0)^3$

For Peer Review Only

Table A2. Non-bonded LJ parameters of alcohols and MEA force fields

Atom	σ (Å)				ϵ (kJ mol^{-1})			
	TraPPE-UA	OPLS	GAFF	MEAa	TraPPE-UA	OPLS	GAFF	MEAa
CH_3	3.75000	—	—	—	0.814415	—	—	—
CH_2	3.95000	—	—	—	0.382444	—	—	—
CH	4.33000	—	—	—	0.083140	—	—	—
C (CH_3)	—	3.50000	3.39967	—	—	0.276144	0.457730	—
C (CH_2)	—	3.50000	3.39967	3.39967	—	0.276144	0.457730	0.457730
C (CH)	—	3.50000	3.39967	—	—	0.276144	0.457730	—
H (CH_3)	—	2.50000	2.64953	—	—	0.125520	0.0656888	—
H (CH_2)	—	2.50000	2.47135	2.47135	—	0.125520	0.0656888	0.0656888
						0.062760 [a]		
H (CH)	—	2.50000	2.47135	—	—	0.125520	0.0656888	—
O (OH)	3.02000	3.12000	3.06647	3.06647	0.773202	0.711280	0.880314	0.880314
		3.07000 [b]						
H (OH)	0.00000	0.00000	0.00000	0.00000	0.000000	0.000000	0.000000	0.000000
N (NH_2)	—	3.30000	3.25000	3.25000	—	0.711280	0.711280	0.711280
H (NH_2)	—	0.00000	1.06908	1.06908	—	0.000000	0.0656888	0.0656888

[a]for CH_2-NH_2 in MEA,

[b]for propylene glycol and glycerol

Table A3. Charge distribution in alcohols and MEA force fields

Atom	Charge (e)			
	TraPPE-UA	OPLS	GAFF	MEAa
CH_3	0.00000	—	—	—
CH_2	+0.26500	—	—	—
CH	+0.26500	—	—	—
C (CH_3)	—	−0.18	−0.23710	—
C (CH_2)	—	+0.145	+0.51200 [a]	0.25000
	—	+0.06 [h]	+0.30500 [b]	0.20000 [h]
	—		+0.18590 [c]	
	—		+0.23950 [d]	
	—		+0.41950 [h]	
C (CH)	—	+0.205	+0.41640	—
H (CH_3)	—	+0.06	+0.05950	—
	—		+0.05980 [c]	—
H (CH_2)	—	+0.06	−0.08060 [a]	0.00000
			−0.00290 [b]	
			+0.00480 [c]	
			−0.02840 [d]	
			−0.00600 [h]	
H (CH)	—	+0.06	−0.03390	—
O (OH)	−0.70000	−0.683	−0.69740 [a]	−0.60000
		−0.73 [c]	−0.73830 [b]	
			−0.76370 [c]	
			−0.69200 [e]	
			−0.69350 [f]	
H (OH)	+0.43500	+0.418	+0.40520 [a]	+0.36000
		+0.465 [c]	+0.43910 [b]	
			+0.46430 [d]	
			+0.43880 [e]	
			+0.42640 [f]	
N (NH_2)	—	−0.9	−1.03480	−0.88000
H (NH_2)	—	+0.36	+0.36000	+0.33500

[a]for ethanol,

[b]for ethylene glycol,

[c]for propylene glycol and glycerol,

[d]for MEA,

[e]for CH_2-OH group in propylene glycol and glycerol,

[f]for CH-OH group in propylene glycol and glycerol,

[h]for CH_2-NH_2 group in MEA

For Peer Review Only

Table A4. Bond lengths for alcohols and MEA force fields

Bond	Bond length (Å)				$10^{-5}k_b$ (kJ mol^{-1} nm^{-2})			
	TraPPE-UA	OPLS	GAFF	MEAa	TraPPE-UA	OPLS	GAFF	MEAa
CH_x - CH_y	1.5400	—	—	—	—	—	—	—
C - C	—	1.5290	1.5350	1.5350	—	—	—	2.5363
C - H	—	1.0900	1.0930	1.0930	—	—	—	2.8108
CH_x - O	1.4300	—	—	—	—	—	—	—
C - O	—	1.4100	1.4260	1.4260	—	—	—	2.6284
O - H	0.94500	0.9450	0.97400	0.97400	—	—	—	3.0928
C - N	—	1.4480	1.4700	1.4700	—	—	—	2.6828
N - H	—	1.0100	1.0180	1.0180	—	—	—	3.2978

Table A5. Angle bending parameters for alcohols and MEA force fields

Angle	θ_0 (^{o})				k_θ (kJ mol^{-1} rad^{-2})			
	TraPPE-UA	OPLS	GAFF	MEAa	TraPPE-UA	OPLS	GAFF	MEAa
CH_x - CH_y - O	109.50	—	—	—	419.03	—	—	—
CH_x - O - H	108.50	—	—	—	460.60	—	—	—
CH_2 - CH - CH_3	112.00	—	—	—	519.63	—	—	—
C - C - C	—	112.700	110.63	—	—	488.273	528.86	—
C - C - O	—	109.500	109.43	109.43	—	418.400	566.51	566.51
C - C - H	—	110.700	110.07	110.07	—	313.800	388.28	388.28
C - O - H	—	108.500	108.16	108.16	—	460.240	394.13	394.13
O - C - H	—	109.500	109.88	109.88	—	292.880	426.77	426.77
H - C - H	—	107.800	109.55	109.55	—	276.144	328.03	328.03
			108.35 [a]				329.70 [a]	
C - C - N	—	109.470	110.38	110.38	—	470.281	553.96	553.96
C - N - H	—	109.500	109.92	116.78	—	292.880	394.13	384.93
N - C - H	—	109.500	109.92	109.92	—	292.880	413.38	413.38
H - N - H	—	106.400	107.13	109.50	—	364.845	345.60	292.88

[a]for CH_3 in ethanol

For Peer Review Only

Table A6. Dihedral torsion parameters for alcohols and MEA force fields (c_i and C_i parameters in kJ mol^{-1})

Dihedral	c_0	c_1	c_2	c_3
TraPPE-UA - Ryckaert-Bellemans dihedral				
CH_3 - CH - O - H	2.51324	5.97851	−0.523117	−5.78388
CH_2 - CH - O - H	2.51324	5.97851	−0.523117	−5.78388
O - CH_2 - CH_2 - O	8.36779	−25.10338	4.183937	33.47117
O - CH_2 - CH - O	8.36779	−25.10338	4.183937	33.47117
TraPPE-UA - Fourier dihedral				
Dihedral	C_1	C_2	C_3	
CH_3 - CH_2 - O - H	3.48736	−0.484826	3.12353	
CH_2 - CH_2 - O - H	3.48889	−0.485039	3.12490	
CH - CH_2 - O - H	3.48889	−0.485039	3.12490	
CH_3 - CH - CH_2 - O	2.93684	−0.886938	12.8024	
OPLS - Ryckaert-Bellemans dihedral				
Dihedral	c_0	c_1	c_2	c_3
C - C - C - H	0.62760	1.88280	0.00000	−2.51040
H - C - C - H	0.62760	1.88280	0.00000	−2.51040
C - C - C - O	2.87441	0.58158	2.09200	−5.54799
C - C - O - H	−0.44350	3.83255	0.72801	−4.11705
O - C - C - O	18.96607	−18.96607	0.00000	0.00000
H - C - O - H	0.94140	2.82420	0.00000	−3.76560
H - C - C - O	0.97905	2.93716	0.00000	−3.91622
O - C - C - N	16.73600	−16.73600	0.00000	0.00000
H - C - C - N	−4.09614	5.08775	2.96645	−3.95806
C - C - N - H	−1.26775	3.02085	1.74473	−3.49782
H - C - N - H	0.83680	2.51040	0.00000	−3.34720
GAFF - Ryckaert-Bellemans dihedral				
Dihedral	c_0	c_1	c_2	c_3
C - C - C - H	0.65270	1.95811	0.00000	−2.61082
H - C - C - H	0.65270	1.95811	0.00000	−2.61082
C - C - C - O	0.65270	1.95811	0.00000	−2.61082
C - C - O - H	1.71544	0.96232	0.00000	−2.67776
O - C - C - O	0.60250	1.80749	9.83240	−2.40998
H - C - O - H	0.69873	2.09618	0.00000	−2.79491
H - C - C - O	1.04600	−1.04600	0.00000	0.00000
O - C - C - N	0.65270	1.95811	0.00000	−2.61082
H - C - C - N	0.65270	1.95811	0.00000	−2.61082
C - C - N - H	1.25520	3.76560	0.00000	−5.02080
H - C - N - H	1.25520	3.76560	0.00000	−5.02080
MEAa - Ryckaert-Bellemans dihedral				
Dihedral	c_0	c_1	c_2	c_3
H - C - C - H	0.65270	1.95811	0.00000	−2.61082
C - C - O - H	0.00000	0.92048	0.00000	1.17152
H - C - O - H	0.69873	2.09618	0.00000	−2.79491
H - C - C - O	1.04600	−1.04600	0.00000	0.00000
O - C - C - N	0.33472	18.77277	−0.66940	−19.34012
H - C - C - N	0.65270	1.95811	0.00000	−2.61082
C - C - N - H	2.46856	15.69000	−4.93712	−13.72352
H - C - N - H	1.25520	3.76560	0.00000	−5.02080

For Peer Review Only

Appendix B: Dynamic response through the dipole moment autocorrelation function

Figure B1. Dynamic response of several organic compounds at 298 K and 1 bar through the Fourier transform of the dipole moment autocorrelation function. For monoethanolamine (MEA), the simulations are performed at 293 K. Solid lines represent the results obtained in our simulations using the different force fields introduced in the text. In the particular case of water, blue, green, magenta, orange and red lines show the results corresponding to the SPC, TIP4P, SPC/E, F-SPC and Fw-SPC models, respectively. For the remaining substances, red, green, blue and magenta lines represent results generated using the TraPPE-UA, OPLS, GAFF and MEAa force fields, respectively. Black circles represent experimental values obtained from Eq. (12) using dielectric spectrum data from different sources for the following systems: water [9–12], ethanol [16–18, 98], ethylene glycol [99], propylene glycol [100], glycerol [96, 97, 101, 102]. For MEA, black open and filled circles are experimental values at 278 K [103] and 308 K [104] respectively.

For Peer Review Only

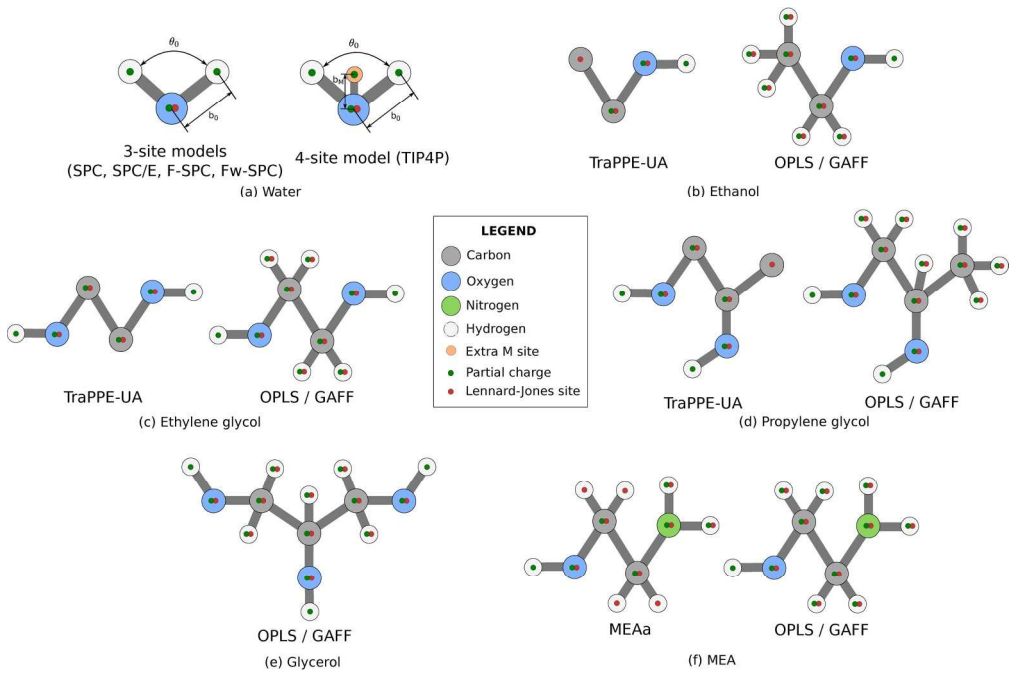

Figure 1. Molecular models used in this study. Carbon, Oxygen, Nitrogen and Hydrogen atoms are represented as grey, blue, green and white circles, respectively. The extra site in the TIP4P water model is shown as a light orange circle. Partial charges appear as dark green dots while Lennard-Jones interaction sites are represented as red dots.
194x128mm (300 x 300 DPI)

For Review Only

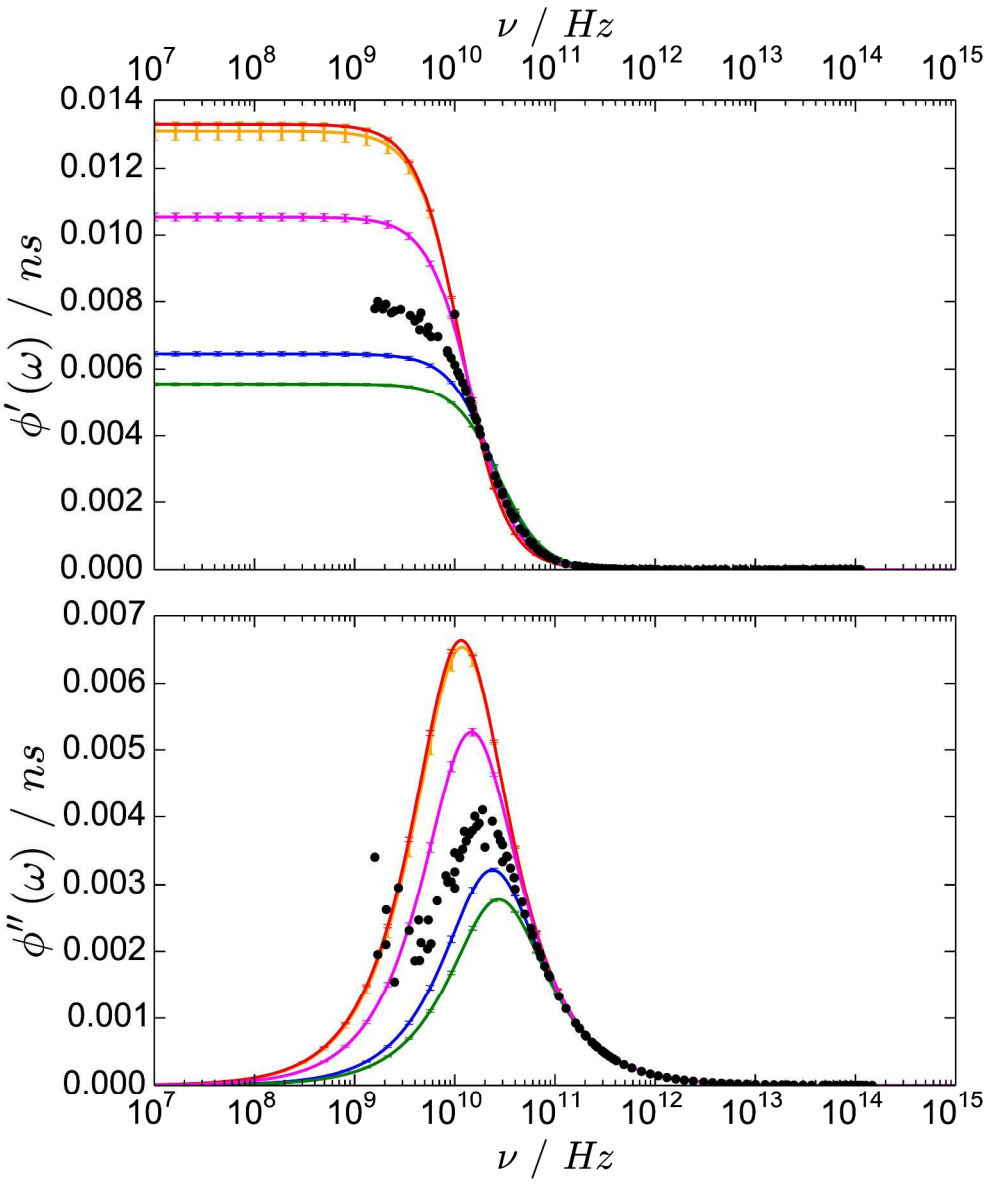

Dynamics of water at 298K and 1 bar through the Fourier transform of the dipole moment autocorrelation function. Blue, green, magenta, orange and red lines show the results corresponding to the SPC, TIP4P, SPC/E, F-SPC and Fw-SPC models, respectively. Black circles represent experimental values obtained from Eq. (12) using dielectric spectrum data from different sources [9-12].
304x365mm (300 x 300 DPI)

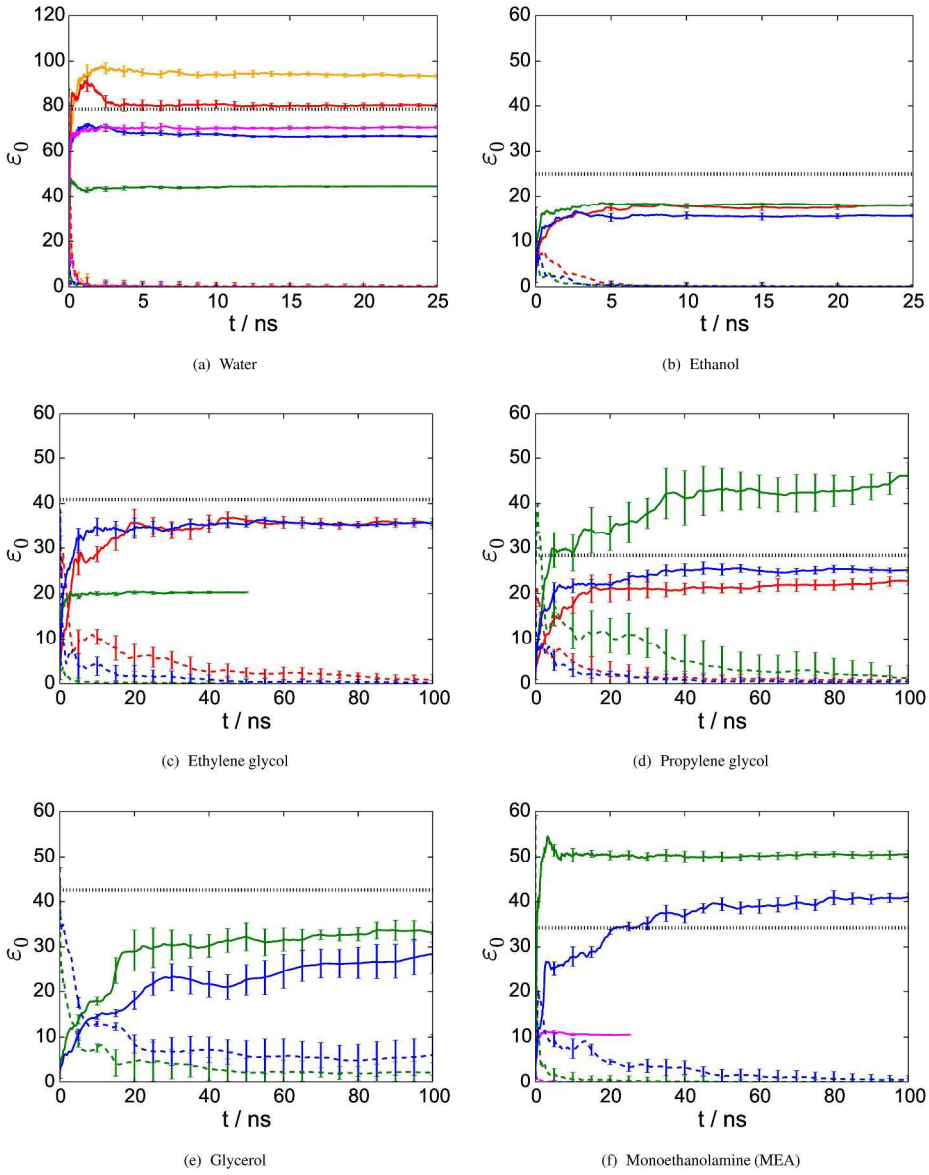

Figure 3. Effect of the block length on the static dielectric constant. The results show running averages started from an energetically equilibrated sample. They are obtained via molecular dynamics simulations at 298K and 1 bar, using Neumann's formula (Eq. 16). For MEA, the simulations are performed at 293 K. Solid lines represent the results obtained using the different force fields introduced in the text. Dashed lines correspond to the term containing the square of the average dipole moment ($\langle M \rangle \cdot \langle M \rangle$) in Eq. 16, which should vanish at long times to consider the static dielectric constant converged. In the particular case of water, blue, green, magenta, orange and red lines show the results corresponding to the SPC, TIP4P, SPC/E, F-SPC and Fw-SPC models, respectively. For the remainder substances, red, green, blue and magenta lines represent results generated using the TraPPE-UA, OPLS, GAFF and MEAa force fields, respectively. Dotted horizontal lines represent experimental values obtained from different sources: water [82], ethanol [76], ethylene glycol [85], propylene glycol [88], glycerol [90] and MEA [92].
264x334mm (300 x 300 DPI)

For Peer Review Only

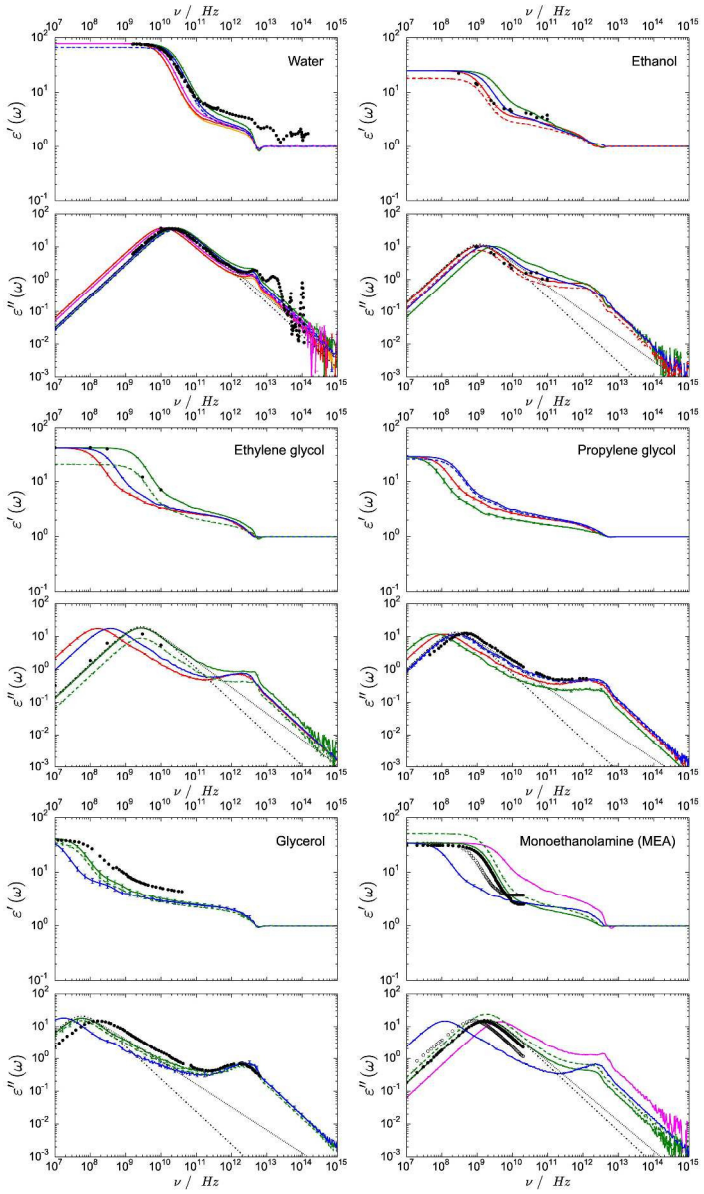

Figure 4. Dielectric response of several organic compounds obtained via molecular dynamics simulations at 298K and 1 bar. For monoethanolamine (MEA), the simulations are performed at 293 K. Solid lines represent the results obtained in our simulations using the different force fields introduced in the text, and employing the experimental static dielectric constant
in the calculations. In the particular case of water, blue, green, magenta, orange and red lines show the results corresponding to the SPC, TIP4P, SPC/E, F-SPC and Fw-SPC models, respectively. For the remaining substances, red, green, blue and magenta lines represent results generated using the TraPPE-UA, OPLS, GAFF and MEAa force fields, respectively. Dashed lines correspond to results using Neumann's formula (Eq. 16) to calculate the static dielectric constant, for the force fields showing a better performance in the prediction of the dielectric spectrum in every case (water SPC, ethanol TraPPE-UA, ethylene glycol OPLS, propylene glycol GAFF, glycerol OPLS and MEA OPLS). Black circles represent experimental values obtained from different sources for the following systems: water [9-12], ethanol [16-18, 97], ethylene glycol [98], propylene glycol [99], glycerol [95, 96, 100, 101]. For MEA, black open and filled circles are experimental

values of the dielectric spectrum at 278K [102] and 308K [103] respectively. Black dot-dash and dotted lines in ε''(ω) represent the fit of the α-relaxation peak to Debye and Cole-Davidson models, respectively.
358x610mm (300 x 300 DPI)

For Peer Review Only

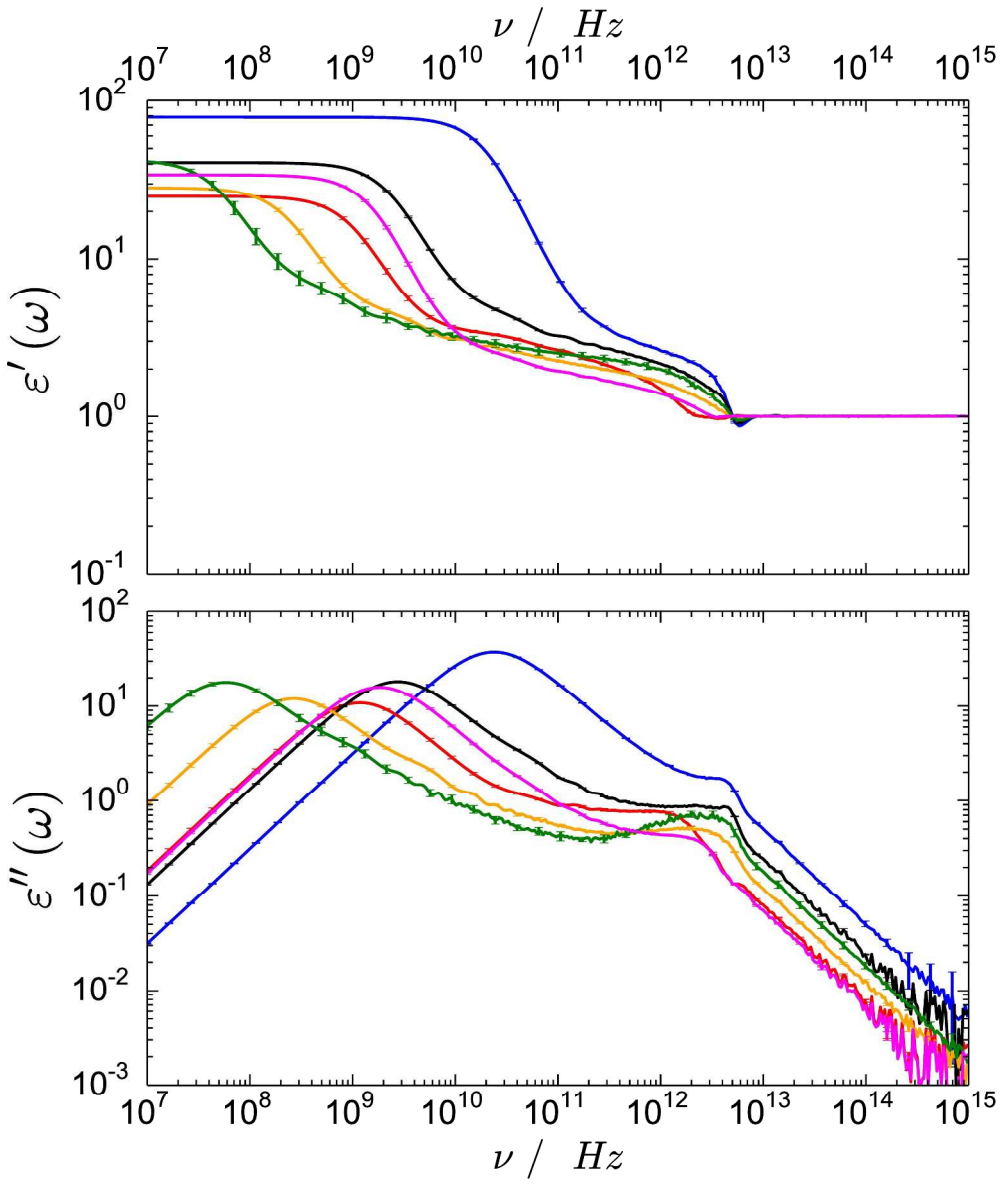

Figure 5. Comparison of the dielectric spectra of different organic substances. The force fields that show a better performance in the prediction of the dielectric response are used in this representation: water SPC (blue), ethanol TraPPE-UA (red), ethylene glycol OPLS (black), propylene glycol GAFF (orange), glycerol OPLS (green) and MEA OPLS (magenta).
304x365mm (300 x 300 DPI)

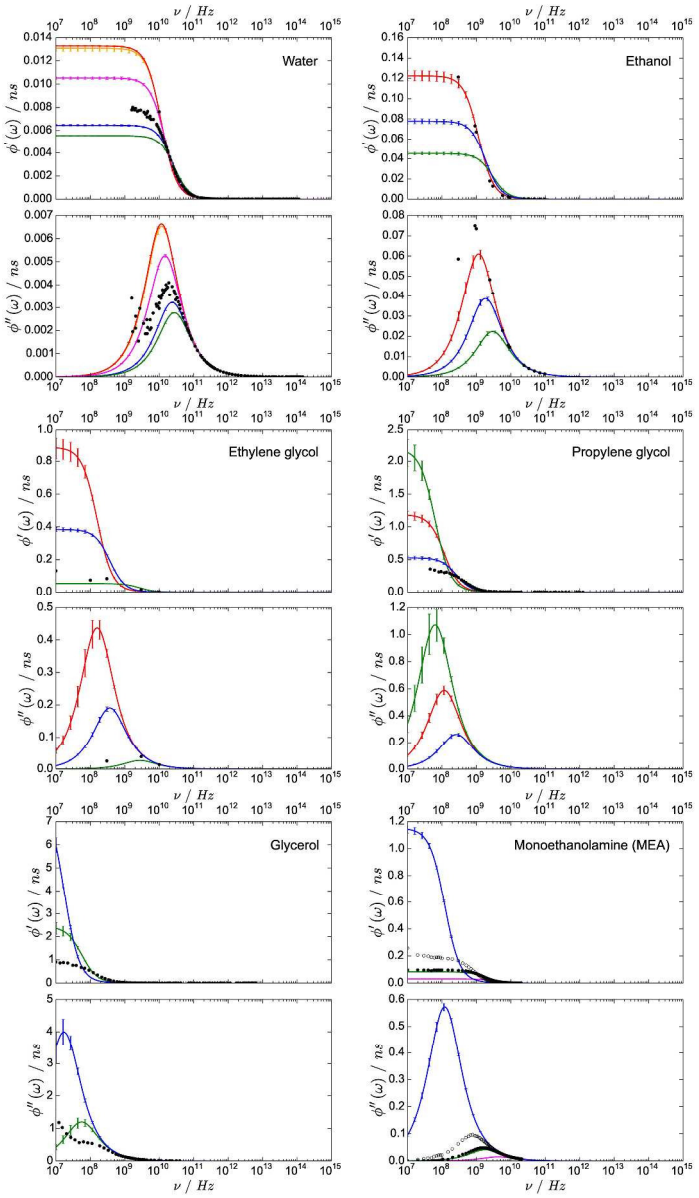

Figure B1. Dynamic response of several organic compounds at 298K and 1 bar through the Fourier transform of the dipole moment autocorrelation function. For monoethanolamine (MEA), the simulations are performed at 293 K. Solid lines represent the results obtained in our simulations using the different force fields introduced in the text. In the particular case of water, blue, green, magenta, orange and red lines show the results corresponding to the SPC, TIP4P, SPC/E, F-SPC and Fw-SPC models, respectively. For the remaining substances, red, green, blue and magenta lines represent results generated using the TraPPE-UA, OPLS, GAFF and MEAa force fields, respectively. Black circles represent experimental values obtained from Eq. (12) using dielectric spectrum data from different sources for the following systems: water [9-12], ethanol [16-18, 97], ethylene glycol [98], propylene glycol [99], glycerol [95, 96, 100, 101]. For MEA, black open and filled circles are experimental values at 278K [102] and 308K [103] respectively.
358x610mm (300 x 300 DPI)